Paroxetine-induced transient apoptosis and delayed neurogenesis act on social behavior in developing zebrafish

Tomomi Sato[1,2]*, Kaito Saito[3], Tsubasa Oyu[3], Sachiko Tsuda[3], Tomohiro Kurisaki[1], Takeshi Kajihara[2], Masabumi Nagashima[1]

[1]Department of Anatomy, School of Medicine, Saitama Medical University, Morohongo 38, Moroyama-machi, Saitama 350-0495, Japan

[2]Department of Obstetrics and Gynecology, School of Medicine, Saitama Medical University, Morohongo 38, Moroyama-machi, Saitama 350-0495, Japan

[3]Division of Life Science, Graduate School of Science and Engineering, Saitama University, 255 Shimo-Okubo, Sakura-ku, Saitama City, Saitama 338-8570, Japan

*Corresponding author

[1]Department of Anatomy, School of Medicine, Saitama Medical University, Morohongo 38, Moroyama-machi, Saitama 350-0495, Japan

Tel: +81-49-276-1148

Fax: +81-49-276-1148

Email: tosato@saitama-med.ac.jp (TS)

Abstract

Autism spectrum disorder (ASD) is a neurodevelopmental condition caused by various genetic and environmental factors. This disorder has the cardinal symptoms including impaired social behavior involving the amygdala. Ingesting antidepressants such as paroxetine in early pregnancy increases the risk of ASD in offspring. However, a comprehensive picture of the underlying pathogenic mechanisms remains elusive. Here we demonstrate that early exposure of zebrafish embryos to paroxetine retards neurogenesis in the optic tectum and the dorsal telencephalon, which corresponds to the human amygdala. Paroxetine-treated embryos exhibit impaired growth, with small heads and short body lengths resulting from transient apoptosis. This is reminiscent of the early-onset fetal growth restriction (FGR) associated with ASD. Interestingly, the delayed neurogenesis in the small heads was found to be restored after the cessation of paroxetine. This restoration was accompanied by extended retinotectal projections, suggesting brain-preferential remodeling. Finally, the paroxetine-treated fish exhibited impaired social behavior, further supporting the correspondence with ASD. Our findings offer new insights into the early neurodevelopmental etiology of ASD.

Introduction

Autism spectrum disorder (ASD) is a neurodevelopmental disorder diagnosed in childhood [1]. The cardinal symptoms include impaired social behavior, communication disorder, and stereotyped repetitive behaviors [2]. To date, a large number of genes have been identified as related to ASD. These are involved in synaptic functions, transcriptional regulation, and brain development [1,3]. Furthermore, de novo mutations, paternal age, maternal infection and inflammation during pregnancy have also been implicated as causative factors [3–5]. Thus, various genetic and environmental factors contribute to the impaired brain development and functions observed in ASD [4–6]. Maternal depression and anxiety during pregnancy are also associated with an increased risk of ASD in offspring [7]. Selective-serotonin reuptake inhibitors (SSRIs), one of the conventional types of antidepressants, are prescribed to pregnant women based on risk-benefit considerations [8]. The drugs act on the maternal brain to exert their therapeutic effects but also pass through the placenta to the fetus [9,10]. Several studies suggest that maternal use of SSRIs during the first trimester of pregnancy increases the risk of ASD [11–14]. However, a comprehensive picture of the underlying pathogenic mechanisms remains elusive.

Fetal growth restriction (FGR) is a common complication during pregnancy and possibly caused by various maternal, placental, and fetal factors [15]. Early-onset FGR manifests as a morphologically symmetrical fetus with a small head and body due to fetal growth failure [16]. The causative factors include genetic abnormalities, congenital malformation, intrauterine infection, and teratogenic effects [15]. This type of FGR is also associated with ASD [17–19]. However, the pathogenesis of ASD and the pathophysiological role of SSRIs in the early-onset FGR is poorly understood.

Serotonin (5-hydroxytryptamine [5-HT]) is a monoamine neurotransmitter involved in emotional disorders such as depression and anxiety by modulating synaptic transmission in the brain [20,21]. SSRIs exert their therapeutic effects by inhibiting the reuptake of 5-HT via serotonin transporter (SERT), to sustain the concentration of extracellular 5-HT [22,23]. 5-HT also plays an important role in adult neurogenesis by promoting the self-renewal of neural stem cells in the hippocampus [24]. Moreover, maternal 5-HT synthesized in the placenta of pregnant mice has been found to transiently localize in the forebrain of early-stage embryos [25], raising the possibility that placenta-derived 5-HT regulates early brain development [26–28]. However, the effects of early-stage SSRI and 5-HT on embryonic brain development and postnatal behaviors are unclear. Elucidation of the primary causes is essential for early prediction

and prevention of the risk for ASD. While SSRI during early pregnancy increases the risk of ASD, the primary cause remains ambiguous [11,13,14]. The involvement of various genetic and environmental factors makes it difficult to comprehensively understand the causes and consequences for the pathogenesis of ASD [1–4]. Thus, there is a need to elucidate the primary actions of SSRI on early brain development and the subsequent effects on social behavior. To address this question, we use zebrafish as a model of human embryos, because easy access to early embryos in a living and intact condition enables us to investigate the direct actions on those embryos. In zebrafish, various models for neurodevelopmental disorders have already been established, suggesting evolutionary conserved pathophysiological mechanisms between humans and zebrafish in the disorders [29–31]. We focus on the SSRI, paroxetine, because of its broad applicability across affective disorders, including major depressive and anxiety disorders [32]. In this study, we assess the effects of paroxetine and compare those with the control and 5-HT, on morphology, neurogenesis, projection in the brain during embryonic, larval stages, and finally on social behavior in juvenile stages.

Results

Amino acids interacting with paroxetine are completely conserved between human and zebrafish SERT

To investigate the effects of paroxetine on brain development in zebrafish embryos, we first examined whether the amino acid sequence of the serotonin transporter (SERT) targeted by paroxetine, is conserved between humans and zebrafish (Fig. 1). Three-dimensional structures of paroxetine-binding sites and interacting amino acids in human SERT have already been well-defined by X-ray crystallography (Fig. 1A) [33,34]. The entire amino acid sequence was 70% identical between the two species (Fig. 1B). All the amino acids that interact with paroxetine at the central site of human SERT were found to be identical between the two species (Fig. 1A, B). We then examined the expression of zebrafish SERT proteins by immunohistochemistry (Fig. 1C and S1 Fig). SERT proteins were weakly but broadly expressed in the brains at 30 hours post-fertilization (hpf), at the time when pet1-positive serotonergic neurons develop in the raphe nuclei (S1 Fig) [35]. We found that SERT proteins were localized to the apical surfaces of radial glial cells in the ventricular zone at 24 hpf, implying that SERT play some roles in neural stem/progenitor cells.

Fig 1. Amino acids interacting with paroxetine are conserved between human and zebrafish SERT. (A) X-ray structure of the ts3 human SERT complexed with paroxetine at the central site (516X, RCSB Protein Data Bank). Amino acids interacting with paroxetine (light blue), indicated in pink. An amino acid forming hydrophobic cavity, indicated in green. (B) Alignments of amino acid sequences of human and zebrafish SERT (P31645 and NP001035061). Amino acids interacting with paroxetine in the central site are completely identical between human and zebrafish. (C) SLC6A4 (SERT) proteins localized in the apical surface of the ventricular zone of the optic tectum (green, open arrowheads). A scheme of the embryonic brain in a dorsal view (Left). The corresponding region shown in the right at high magnification is indicated (Bold rectangle). A scheme of an RFP-expressing radial glial cell and the SLC6A4 localization is shown (Right).

Early transient paroxetine generates embryos with a short body and a small head which is restored at later larval stages

To clarify the effects of paroxetine on embryonic development, we treated embryos with paroxetine and the effector 5-HT between 26–50 hpf, which roughly corresponds to the

first trimester of human embryos (Fig. 2A) [36]. To determine subthreshold concentrations appropriate for treatment, we treated embryos and calculated survival rates at different concentrations of paroxetine and 5-HT. Both compounds had no effect on the survival rate at less than 20 μM (Fig. 2B). Then, we measured the head-tail body length and head area of paroxetine-treated embryos to parallel the indication of human fetal development estimated by crown-lump length (CRL) between weeks 8–11 of the first trimester in human pregnancy [37]. At first, we monitored the typical development of wild-type embryos. In these experiments, body lengths and head areas were gradually but significantly greater than those embryos at 50 hpf according to developmental stages (S2 Fig). We found that embryos treated with 10 μM paroxetine exhibited restricted growth with a slight but significant decrease in body length and head area at 50 hpf, whereas no significant decreases were detected in embryos treated with 1 μM paroxetine (Fig. 2C–E). This closely resembled early-onset FGR of human embryos in the first trimester [16]. In contrast, 5-HT did not affect both the body length and head area of the embryos at the concentrations of 10 μM and 1 μM, indicating that the observed embryonic growth restriction is a paroxetine-selective action (Fig. 2C–E). Embryos treated with 1 μM paroxetine for two days exhibited significantly shorter body lengths and smaller head areas at 73 hpf (S3 Fig). In addition, treatment with 10 μM

paroxetine for one day had a similar effect on larval morphology at 3 dpf, suggesting that transient early-stage treatment is sufficient for paroxetine to exert its growth-inhibiting effects (S3 Fig). Therefore, we investigated the effects of early transient paroxetine on later development. 5-dpf larvae treated with 10 μM paroxetine during 26–50 hpf showed significant decreases in body lengths and head areas compared to the controls (S4 Fig). Interestingly, the paroxetine-treated larvae exhibited restoration of their head areas compared to the controls at 7 dpf despite persistent decreases in their body lengths (Fig. 2F–I). This observation implied that brain-preferential remodeling occurrs between 5–7 dpf.

Fig 2. Early paroxetine induces embryonic growth restriction followed by preferential restoration in the head at a larval stage. (A) A scheme for the time course of treatment. (B) Dose-responses of survival rates for paroxetine- (blue) and 5-HT- (magenta) treated embryos. (C) Lateral views of 50-hpf zebrafish embryos treated with parox, 5-HT, or the control DMSO. (D, E) Quantification of the body lengths (D) and head areas (E) of the treated embryos. A representative image of an embryo indicating the quantified body length (black line, D) and head area (dotted line, E) are shown in the bottom. (F) Scheme for the treatment schedule and major events in

zebrafish development. (G) Lateral views of 7-dpf larvae treated with parox, 5-HT, or DMSO. (H, I) Quantification of the body lengths (H) and head areas (I) of the treated embryos. A representative image of a larva indicating the quantified body length (black line, H) and head area (dotted line, I) in the bottom.

Paroxetine but not 5-HT transiently induces local apoptosis in the head and tail tip

To elucidate the mechanisms underlying the different effects of paroxetine and 5-HT on embryonic growth and development, we examined the induction of apoptosis at 31 hpf, 5 hours after treatment with paroxetine or 5-HT by immunostaining with an antibody against active Caspase-3 (Fig. 3A, B). We found a significant increase in the immunofluorescent signals of active Caspase-3 in the brain of paroxetine-treated embryos compared to the control dimethyl sulfoxide (DMSO)-treated embryos (Fig. 3B, D, parox). The apoptosis induced by paroxetine was increased in a dose-dependent manner (Fig. 3E). In contrast, no such increase was detected in 5-HT-treated embryos (Fig. 3B, D, 5-HT). This is consistent with our observations that 5-HT had no effects on the head area (Fig. 2C, E). Co-treatment of paroxetine with 5-HT also increased apoptosis in the brain, suggesting that the apoptosis is directly induced by paroxetine

blocking the incorporation of 5-HT via SERT, but not through extracellular 5-HT (Fig. 3F). Moreover, in addition to the apoptosis in the brain, apoptosis was also induced locally in the tail tip of paroxetine-treated embryos in an almost all-or-nothing manner (Fig. 3C, G). Consistent with paroxetine-treated embryos, *slc6a4a* (*serta*)-knockdown embryos also exhibited growth restriction in the body length and increased apoptosis in the brain were observed in (S1 Fig). These results indicate that the increased apoptosis was caused by reduced 5-HT transportation due to the inhibition or knockdown of SERT. Thus. the local apoptosis in the brain and the tail tip corresponded to the growth restriction of the paroxetine-treated embryos with decreased head area and body length (Fig. 2C–E). Next, we examined whether apoptosis persistently occurred in the paroxetine-treated brain at 48 hpf. The Caspase-3-positive signals were significantly decreased in the optic tecta (OT) and the telencephalons (T) of paroxetine-treated embryos, indicating that apoptosis acutely induced after the treatment was suppressed in the brains at later stages (Fig. 3H–J).

Fig 3. Paroxetine transiently induces local apoptosis in the brain and tail tip of treated embryos. (A) A scheme for the time course of treatment. (B) Lateral views of the heads of 31-hpf embryos treated with DMSO, parox, or 5-HT and immunostained

for active Caspase-3 (white puncta). Images binarized above a threshold. Dotted line: Morphological outlines. (C) Lateral views of the tail tips of 33-hpf embryos treated with DMSO, parox, or 5-HT and immunostained for active Caspase-3. Anterior, left; posterior, right. (D–G) Quantification of the mean intensities of active Caspase-3 signals in the heads (D–F) and tail tips (G). (H) Lateral views of DMSO- or parox-treated embryos immunostained for active Caspase-3 (white puncta) at 48 hpf. Images binarized above a threshold. Dotted line: Morphological outlines. (I, J) Quantification of the mean intensities of active Caspase-3 in the optic tecta (I) and telencephalons (J) of the treated embryos. Scale bars: 100 μm (B, C, H). Data are presented as mean ± SEM. $*p < 0.05$, $**p < 0.01$, $****p < 0.0001$; ns, not significant. Kruskal-Wallis with Dunn's multiple comparisons tests; parox, paroxetine; 5-HT, serotonin; DMSO, dimethylsulfoxide; hpf, hours post-fertilization; parox, paroxetine; SEM, standard error of the mean. OT, optic tectum; T, telencephalon.

Paroxetine suppresses neurogenesis in the optic tectum during an increase in proliferation of neural progenitor cells

We then explored the effect of paroxetine on neurogenesis in the optic tectum, since it has been well defined as a visuomotor center in the zebrafish brain in terms of the

development and function of the neural circuits [31, 38–42]. For this purpose, we used transgenic lines TgBAC(*neurod1:EGFP*), expressing enhanced green fluorescent protein (EGFP) in differentiated neurons [43], and Tg(*elavl3:kaede*), expressing Kaede under a pan-neuronal promoter *elavl3* (*huC*) [44] (Fig. 4A and S4 Fig). To evaluate the effect on neurogenesis by treatment with paroxetine and other small-molecule compounds using intact whole embryos, we examined fluorescence-positive area and the fluorescence intensity to establish simple indicators of the number of post-mitotic neurons expressing a fluorescent protein such as EGFP or Kaede. Previously we have revealed that GFP intensity in post-mitotic neurons increases with developmental stages, because it is proportional to the number and the time after differentiation of those neurons [31]. Imaging and relative quantification processes are shown in S4 Fig and Materials and Methods. We found that the EGFP and Kaede fluorescence in post-mitotic neurons were significantly decreased in the optic tectum and the telencephalon by the treatment with paroxetine during 26–50 hpf compared to the control (Fig. 4A–C and S3 Fig). Indeed, the number of EGFP-positive neurons (with intensity above 70) in the optic tectum was significantly decreased in paroxetine-treated embryos, indicating that neurogenesis was suppressed by paroxetine at 50 hpf (Fig. 4D). To examine whether the effect of paroxetine on neurogenesis is mediated by the upregulation of extracellular

5-HT, we treated embryos with 5-HT during the same developmental stages. Consistent with the paroxetine-treated embryos, EGFP fluorescence was significantly decreased in the optic tectum of 5-HT-treated embryos compared to the controls, indicating that the effect of paroxetine is recapitulated by 5-HT (Fig. 4E, F).

In adult neurogenesis of both rodents and humans, SSRIs are known to promote the proliferation of neural stem cells [24,45]. Then, we examined the proliferation of neural stem/progenitor cells in the optic tectum by immunostaining with anti-phospho-histone H3 (pH3) antibody to label mitotic cells [31]. We found that paroxetine-treated embryos showed an increase in the number of pH3-positive mitotic cells at 50 hpf (Fig. 4G, H). The increase was selectively observed in the subventricular zone (SVZ) where cell divisions of intermediate progenitor cells occur for neurogenesis and proliferation (Fig. 4G, I, J) [46]. Expression of SOX2, a marker of proliferating neural stem/progenitor cells, was enhanced in paroxetine-treated embryonic brains, with a concomitant decrease in Kaede expressing neurons at 48 hpf, although an increase in *sox2* mRNA expression was not detected by RT-qPCR with whole embryos [47] (S3 Fig). These results suggest that paroxetine promotes the proliferation of neural stem/progenitor cells by suppressing neurogenesis in the optic tectum.

Fig 4. Paroxetine suppresses neurogenesis and promotes proliferation of neural progenitor cells in the optic tectum. (A) Representative 50-hpf TgBAC(*neurod1:EGFP*) embryos treated with parox and the control DMSO shown in lateral views. EGFP-positive region in the optic tectum (dotted ellipse) for quantification is indicated (arrowhead). (B) Intensity frequency of the EGFP-positive region in the optic tectum of DMSO- (top) and paroxetine- (bottom) treated embryos (DMSO, 24.38 ± 1.359 pixels; Parox, 21.30 ± 0.882 pixels; each n = 5). (C) Quantification of the mean EGFP intensity in the optic tectum (dotted ellipse with arrowheads in A). Unpaired t test. (D) Quantification of the number of EGFP-positive neurons with intensity above 70 in the optic tectum. (E) Lateral views of 50-hpf TgBAC(*neurod1:EGFP*) embryos treated with parox, 5-HT, and the control DMSO. (F) Quantification of the mean EGFP intensity in the optic tecta (arrowheads in E) of the embryos. Kruskal-Wallis with Dunn's multiple comparisons tests. (G) High-magnification images of the optic tecta of zebrafish embryos treated with DMSO or parox and immunostained for pH3 (red), with DAPI (blue) co-staining for the nuclei. Open arrowheads, pH3-positive cells in the SVZ. (H–J) Quantification of the number of pH3-positive cells in the optic tecta (H), the ventricular zones (I), and the subventricular zones (J). Scale bars: 100 μm (A, E); 25 μm (G). Data are presented as mean ± SEM. *p

< 0.05, $^{**}p < 0.01$, $^{***}p < 0.001$; ns, not significant. Mann-Whitney U test; 5-HT, serotonin; Cb, cerebellum; DAPI, 4′,6-diamidino-2-phenylindole fluorescent stain; DMSO, dimethylsulfoxide; e, eye; EGFP, enhanced green fluorescent protein; H, hindbrain; hpf, hours post-fertilization; OT, optic tectum; parox, paroxetine; pH3, phospho-histone H3; SEM, standard error of the mean; SVZ, subventricular zone; T, telencephalon; VZ, ventricular zone.

The development of retinotectal projections is impaired by early transient paroxetine and later restored with extended retinal axons

To investigate whether the suppressed neurogenesis in the brain of paroxetine-treated embryos impacts later neural circuit formation, we examined the retinotectal projections. We used transgenic line Tg(*pou4f1-hsp70l:GFP*) expressing GFP in excitatory tectal neurons and retinal ganglion cells (RGCs), and line Tg(*pou4f3:GAL4;UAS:mCherry*) expressing mCherry in RGCs [43,44]. In wild-type larvae, GFP- and mCherry-expressing areas gradually and significantly increased with developmental stages in the optic tecta compared with those areas at 72 hpf (S2 Fig). In contrast, the fluorescence of both the GFP and mCherry-expressing areas was significantly decreased

between 5 and 7 days post fertilization (dpf) during which activity-dependent competition followed by dynamic synapse formation or elimination occurs in retinal axons and tectal dendrites, respectively (S2 Fig) [38,39]. Treatment with 1 μM paroxetine for two days caused significant decreases in both the area and the fluorescence of the region expressing GFP and mCherry in the optic tectum at 73 hpf (Fig. 5A–E). One-day treatment with 10 μM paroxetine also showed a similar effect on the GFP-expression region (S3 Fig). Thus, transient early-stage treatment of paroxetine is responsible for suppressing the development of the retinotectal projections, consistent with the growth-inhibiting effects on larval morphology (S3 Fig). Therefore, we examined the effects of the early transient paroxetine on later development of the retinotectal projections. In accordance with the restoration of the head area at 7 dpf (Fig. 2G, I), paroxetine-treated 7-dpf larvae exhibited restoration of both the area and the fluorescence of the GFP-expressing region and the fluorescence of the mCherry-expressing region in the optic tectum by reverting the values to those in the controls (Fig. 5F–H, J). Furthermore, the areas of mCherry-expressing regions were significantly expanded in paroxetine-treated larvae compared to the controls (Fig. 5I, parox). This expansion was recapitulated in 5-HT-treated larvae (Fig. 5I, 5-HT), suggesting that early transient paroxetine drives the extension of retinal axons through

5-HT at later neurodevelopmental stages.

Fig 5. Early transient paroxetine inhibits the development of the retinotectal projection leading to brain-preferential remodeling. (A) Lateral views of the heads of 73-hpf Tg(*pou4fl-hsp70l:GFP; pou4f3:GAL4;UAS:mCherry*) embryos treated with DMSO or parox at 1 μM for 2 days from 26 hpf. Tectal neurons and retinal axons express GFP (green) and retinal axons express mCherry (magenta). (B) Quantification of the GFP-positive areas. (C) Mean GFP intensities in the optic tecta of the transgenic embryos. (D) Quantification of the mCherry-positive areas. (E) Mean mCherry intensities in the optic tecta of the transgenic embryos. A representative image indicating the quantified area (dotted line) in the optic tectum are shown (B, D, top insets). Mann-Whitney U test. (F) Lateral views of the heads of 7-dpf Tg(*pou4fl-hsp70l:GFP;pou4f3:GAL4;UAS:mCherry*) larvae treated with parox, 5-HT, or the control DMSO. Optic tecta (filled arrowheads) and retinal axons (open arrowheads). (G–J) Quantification of the GFP-positive areas (G), the mean GFP intensities (H), the mCherry-positive areas (I), and the mean mCherry intensities (J) in the optic tecta of the transgenic larvae. Kruskal-Wallis with Dunn's multiple comparisons tests; Scale bar, 100 μm. Data are presented as mean ± SEM. *$p < 0.05$,

**$p < 0.01$; ns, not significant. 5-HT, serotonin; DMSO, dimethylsulfoxide; GFP, green fluorescent protein; hpf, hours post-fertilization; parox, paroxetine; SEM, standard error of the mean.

Early paroxetine negatively impacting neurogenesis in the dorsal telencephalon affects typical development of social behavior

Next, we investigated whether the early paroxetine treatment affects the development of the dorsal telencephalon, which corresponds to the mammalian amygdala [29]. The amygdala plays a critical role in social behavior. Amygdala dysfunction causes impaired social behavior characteristic of ASD [2]. To assess the effects of paroxetine, SAGFF120A gene-trap line was used, because the line locally expresses Gal4FF in neurons of the dorsal telencephalon which are essential to active avoidance fear conditioning [49]. Fluorescence of the GFP-expressing areas was significantly decreased in the dorsal telencephalons of paroxetine- and 5-HT-treated embryos compared to the control at 48 hpf (5-HT, $p = 0.00161$, Fig. 6A, B), and 76 hpf (parox, $p = 0.0279$; 5-HT, $p = 0.0250$, S6 Fig), as observed in the optic tecta. Consistently, the GFP fluorescence in the dorsal telencephalon was restored at 7 dpf following washout

of paroxetine and 5-HT at 2 dpf (Parox, $p = 0.1419$; 5-HT, $p = 0.6623$; Fig. 6C–F). This restoration concomitantly occurred with that in the head area, corresponding to the results observed in the larval optic tecta (Fig 2I, Fig. 5F, H, J, S6 Fig).

Finally, we explored whether these neurodevelopmental effects of early transient paroxetine have an impact on juvenile social behavior. To assess social behavior of a young fish, we developed a behavioral apparatus using a test case separated into three chambers: a test area, a sibling area, and a non-sibling area (Fig. 7A; see Methods). The swimming trajectories of the fish in the test area were recorded in the absence (non-sibling trial) or presence (sibling trial) of siblings in the sibling area. We examined which area the fish was located in the sibling (blue) or non-sibling area (red) per frame to determine whether the fish show a social preference for the sibling frame. This was measured by calculating the social preference index (SPI, $-1 < SPI < 1$) (Fig. 7B, C; S1–S6 Videos; see Methods) [50]. Our behavioral analysis revealed that the incidence of positive SPI (sibling trial > non-sibling trial, white) was lower in the fish treated with paroxetine and 5-HT than in the control fish. In contrast, the incidence of negative SPI (sibling trial < non-sibling trial, black) was increased in the paroxetine- and 5-HT-treated fish compared to the control (Fig. 7D; DMSO, n = 13; parox, n = 7; 5-HT, n = 6). Indeed, each value of the SPI difference between the sibling and non-sibling

trials tended to be more negative both for paroxetine and 5-HT than the control (Fig. 7E). These results indicated a tendency for impaired social behavior. On the other hand, we found a difference in the effect on total swimming distance between paroxetine and 5-HT. Total distances of swimming trajectories were always shorter in the sibling trials, producing negative values for differences between sibling and non-sibling trials in the control (Fig. 5F). The decrease in the total distances in the sibling trials were also observed in paroxetine-treated fish, whereas a significant increase in those total distances was observed in the 5-HT-treated fish compared to the control and paroxetine (control, $p = 0.0427$; parox, $p = 0.0082$; Fig. 5F). These results indicated a difference in the effects on social behavior by early transient exposure between paroxetine and 5-HT.

Fig 6. Early transient paroxetine exerts suppressive effects on neurogenesis followed by restoration in the dorsal telencephalon. (A) Dorsal views of 48-hpf SAGFF120A;UAS:GFP zebrafish embryos treated with parox, 5-HT, or DMSO (control). (B) Quantification of the mean GFP intensities in the dorsal telencephalons of SAGFF120A;UAS:GFP zebrafish embryos. Kruskal-Wallis with Dunn's multiple comparisons tests. (C) Dorsal views of 7-dpf SAGFF120A;UAS:GFP larvae treated with paroxetine. (D) Dorsal views of 7-dpf SAGFF120A;UAS:GFP larvae treated with

5-HT. (E) Quantification of the mean GFP intensities in the dorsal telencephalons. p = 0.1419, Mann-Whitney U test. (F) Quantification of the mean GFP intensities in the dorsal telencephalons. p = 0.6623, Mann-Whitney U test. Scale bar, 100 μm. Data are presented as mean ± SEM. *$p < 0.05$, ***$p < 0.001$; ns, not significant. 5-HT, serotonin; DMSO, dimethylsulfoxide; GFP, green fluorescent protein; hpf, hours post-fertilization; parox, paroxetine; SEM, standard error of the mean.

Fig 7. Early transient paroxetine- and 5-HT-treated zebrafish exhibit atypical social behavior. (A) A test case used in this study. The sibling frame shown in blue, the non-sibling frame shown in red. (B) Representative swimming trajectories of the fish treated with DMSO (control), parox, or 5-HT in the non-sibling (top) and sibling trials (bottom). The SPIs indicated below. (C) A total of 2,998 frames recorded over 5 min for the trials shown in (B) with color-coded according to the frames in (A). (D) Incidences of positive SPI (sibling > non-sibling, white) and negative SPI (sibling < non-sibling, black) in the fish treated with DMSO, parox, and 5-HT (n = 13, 7, 6, respectively). (E) Differences in SPIs between the sibling and non-sibling trials. Data are presented as mean ± SEM, p = 0.0456, Brown-Forsythe ANOVA test. (F) Differences in the total swimming trajectory distances of the fish between the sibling and non-sibling trials.

Data are presented as mean ± SEM, *$p < 0.05$, **$p < 0.01$; ns, not significant. Brown-Forsythe with Dunnett's multiple comparisons tests. 5-HT, serotonin; ANOVA, analysis of variance; DMSO, dimethylsulfoxide; GFP, green fluorescent protein; hpf, hours post-fertilization; parox, paroxetine; SEM, standard error of the mean; SPI, social preference index.

Discussion

In this study, we show that early exposure to paroxetine restricts embryonic growth, resulting in short body lengths and small heads in zebrafish. In humans, early-onset FGR manifests as symmetrical morphology with a small head and body, and the causative factors include teratogenic effects [15,16]. Thus, the paroxetine-treated zebrafish embryos are considered as a model of early-onset FGR in humans. The growth restriction is induced by paroxetine but not by 5-HT which is incorporated into cells through SERT, the target protein blocked by paroxetine. Consistently, apoptosis is locally induced by paroxetine in the brain and the tail tip, but not by 5-HT, suggesting that apoptosis is the underlying mechanism for the paroxetine-induced embryonic growth restriction. However, these results imply disparities between the effects of

paroxetine and 5-HT on embryogenesis. SSRIs including paroxetine have already been reported to induce apoptosis in various malignant cell types, including gliomas, neuroblastomas, leukemia, lymphomas, and colon tumors, in addition to normal cells such as myeloid cells, osteoblasts, and osteoclasts [51–54]. These lines of evidence suggest a shared mechanism of action of SSRIs for the apoptosis induction in proliferating cells, potentially attributable to the etiology of adverse effects of SSRIs on embryogenesis. In addition, another SSRI, fluvoxamine, has recently been identified that have therapeutic potential as an immunomodulator due to its ability to suppress immune responses which is likely to reduce the risk of deterioration in COVID-19 [55,56]. These pleiotropic effects of SSRIs are reminiscent of those of thalidomide. Thalidomide also has proapoptotic properties to exert the teratogenic effects on embryogenesis, and the exposure during early pregnancy has been associated with ASD in the offspring [57,58]. Furthermore, the thalidomide derivatives are therapeutically used as immunomodulatory drugs [59,60]. Taken together with those studies, our findings imply a shared common mechanism underlying teratogenic and therapeutic effects of SSRI which are related to the pathogenesis of ASD.

Here, we reveal that paroxetine- and 5-HT-treated embryos exhibit suppressed neurogenesis in the optic tectum. Despite those effects on neurogenesis, the number of

pH3-positive mitotic cells are selectively increased in the subventricular zone. These observations suggest that the proliferation of neural stem/progenitor cells is promoted by paroxetine, because neurons are generated from neural stem/progenitor cells at the expense of the proliferation of those cells during brain development [31,61]. This is supported by increased expression of SOX2, a marker of proliferating neural stem/progenitor cells in the brain [62]. Our observations are consistent with the effect of SSRI that increases the number of neural stem/progenitor cells in the dentate gyrus of the adult mammalian hippocampus through the increased concentration of 5-HT [24,45,63]. Our results also suggest the biological mechanisms that underlie, while SSRI ingestion during pregnancy have therapeutic effects on the maternal brain, it has adverse effects on the fetal brain development in humans [11–14]. Indeed, we show that apoptosis is transiently induced and thereafter decreased in the brain, which generates growth restriction of paroxetine-treated embryos. These observations are consistent with a previous report showing that SERT-knockout mice exhibit reductions in programmed cell death in the brain [64].

Intriguingly, we find that the head size is restored at a later larval stage in early paroxetine-treated embryos, whereas body length is not, implying brain-preferential remodeling. Likewise, we prove that the suppressed neurogenesis in the optic tectum

decreases the areas and the fluorescence in the retinotectal projection of the paroxetine-treated embryos, which are later restored after the removal of paroxetine. These observations raise the possibility that remodeling occurs in neural networks in the larval brains during the restoration processes, because the remodeling period corresponds to the activity-dependent refinement stages in the retinotectal projection [38,39]. Indeed, we reveal extended projections of retinal axons in the restored brain. This phenotype in axonal projections is similar to that observed in SERT-knockout mice which exhibit impaired segregation of retinal axons both in the superior colliculus and the dorsal lateral geniculate nucleus, leading to the disruption of sensory map formation [65,66]. Those extended axons are also observed in the optic tecum treated with 5-HT. Similarly, the suppressed neurogenesis is also detected in both the optic tecta treated with paroxetine and 5-HT. Thus, our findings suggest that suppressed neurogenesis is a cause of extended axonal projections, because those projections are observed regardless of whether growth restriction and local apoptosis are induced by the treatments. This provides insight into a biological basis for the neurodevelopmental disorders associated with early-onset FGR. The suppressed neurogenesis followed by the restoration is also observed in the dorsal telencephalon treated with paroxetine and 5-HT using the gene-trap line SAGFF120A. In the gene-trap line, neurons in the dorsal telencephalon

corresponding to the mammalian amygdala are visualized by GFP. These neurons have been identified that play a critical role in active avoidance fear conditioning [29,49]. Therefore, the restoration in the dorsal telencephalon implies that the treatments cause remodeling similarly to the optic tectum, which affects the neural circuit function involved in fear conditioning. Indeed, in individuals with ASD, the number of neurons in the amygdala has been found not to undergo neurotypical alterations during their development [67].

Finally, we elucidate the impacts of suppressed neurogenesis on the development of social behavior. In the control fish, the SPI differences between sibling and non-sibling trials vary among individuals, and thereby these are no significant difference in paroxetine- and 5-HT-treated fish as compared with the control. However, the incidence of negative SPI is markedly increased in both the treated fish. Thus, our behavioral analyses demonstrate the negative impact of early exposure to paroxetine and 5-HT on the development of social behavior, albeit with a broad spectrum of their impacts. This implies that the suppressed neurogenesis can be at risk for neurodevelopmental disorders, even when that is induced by other genetic or environmental factors. Of note, the effects on total swimming distance are significantly different between paroxetine and 5-HT, implying a difference in the effects on neural circuits involving social

behavior. These findings offer new insights into the neurodevelopmental mechanisms underlying the pathogenesis of ASD. However, a more detailed analysis is a prerequisite for fully understanding the difference in the effects of paroxetine and 5-HT on the structure and function of the relevant neural circuits. Nevertheless, our study provides evidence for the effects of early transient paroxetine and 5-HT on embryonic brain development and their consequences on social behavior. Furthermore, it will also provide a potential simple screening system for evaluating risk factors for ASD and neurodevelopmental disorders affecting social behavior using zebrafish.

Methods

Zebrafish maintenance and strains

Wild-type and transgenic zebrafish were kept at 28ºC under 14 hours:10 hours light/dark cycles as described previously [68], in an IWAKI Small fish breeding unit LAbREED ITS. To obtain transgenic embryos, a wild-type strain Riken WT (RW) was crossed with transgenic lines as follows: Tg(*elavl3:Kaede*) to visualize post-mitotic neurons [44]; TgBAC(*neurod1:EGFP*) to visualize differentiated neurons[43];

Tg(*pau4f1-hsp70l:gfp*) to visualize development of post-mitotic excitatory neurons and retinal axons in the optic tectum [40]; Tg(*pau4f3:GAL4;UAS:mCherry*) to visualize retinal axons in the optic tectum [48]; and SAGFF120A;UAS:GFP to visualize neurons in the dorsal telencephalon [49]. All embryos and larvae were maintained at 28ºC in E3 embryo medium (5 mM NaCl, 0.17 mM KCl, 0.33 mM MgSO4, 0.33 mM CaCl2), then E3 medium containing 0.003% 1-phenyl 2-thiourea (PTU) from approximately 8 hpf, and those media were refreshed daily. Embryos and larvae were removed from their chorions, used at the stage noted in each experiment, then anesthetized with MS-222 in the medium immediately before fixation. All animal experiments for this study were approved by the Animal Experimentation Committee of Saitama Medical University (No. 3993) and performed in accordance with the Regulation on Animal Experimentation at Saitama Medical University.

Microinjection

Preparation and injection of antisense morpholino oligonucleotides (MOs) were carried out as previously described [31]. Briefly, MOs were diluted in 1× Danieau buffer (58 mM NaCl, 0.7 mM KCl, 0.4 mM MgSO4, 0.6 mM Ca(NO3)2, 5.0 mM HEPES, pH 7.6) and injected into 1 to 2-cell-stage embryos by using a microinjector FemtoJet 5247

(Eppendorf). The sequences and the concentrations of MOs (Gene Tools, OR, USA) used in this study are as follows: slc6a4a-AMO (splice-blocking antisense MO, MO1-slc6a4a, ZDB-MRPHLNO-141031-1, ZIRC) [69], 5'-ACGCACTTACATGCACTTACACATA -3', at 4.178 ng/nl; slc6a4a-5mis (5mis; 5-bp-mismatched control), 5'- ACCCACTTAGATCCAGTTAGACATA -3', at 4.198 ng/nl.

Drug treatments

Preparation of paroxetine and 5-HT solution were carried out as described previously [47]. Briefly, paroxetine (P1977, Tokyo Chemical Industry (TCI), Tokyo, Japan) or 5-HT (S0370, TCI, Tokyo, Japan) were dissolved in dimethyl sulfoxide (DMSO) (Nacalai Tesque, 13407-45, Kyoto, Japan) at 10 mM for stock solutions and diluted with E3 medium to adjust the final concentration from 1 or 20 μM in 1% DMSO. Zebrafish embryos were dechorionated with forceps and immersed in the solution from 26-27 hpf, and then incubated at 28.5ºC. Most of embryos treated under these conditions were survived (see Fig. 2B), and those embryos were euthanized for further analyses or after social behavioral analysis.

Immunohistochemistry

Whole-mount immunohistochemistry was carried out as previously described [31]. Briefly, embryos were fixed with 4% paraformaldehyde/PBS and incubated with primary antibodies at 4ºC overnight, followed by incubation with secondary antibodies against rabbit or goat IgG conjugated with Alexa Flour 488 or 555 (Abcam, Cambridge, UK) together with DAPI (Thermo Fisher Scientific, MA, USA). The following primary antibodies were used in this study: anti-active Caspase-3 (rabbit, 1:500 dilution, 559565, BD Pharmingen, NJ, USA); anti-phospho histone H3 (pH3; 1:500 dilution, 9701, Cell Signaling, MA, USA); Sox2 (rabbit, 1:500 dilution, GeneTex GTX124477); anti-Serotonin (goat, 1:500 dilution, ab66047, Abcam, Cambridge, UK); SLC6S4/5-HTT (rabbit, 1:100 dilution, PA5-49572, Thermo Fisher Scientific, MA, USA). Following immunostaining, phosphate-buffered saline (PBS), the wash solution of embryos was gradually substituted by 30%, 50% and finally 70% glycerol/PBS for imaging under a microscope.

RNA extraction and RT-qPCR

Total RNAs were extracted from whole embryos injected with MOs or treated with drugs using miRNeasy mini prep kit according to the manufacture's protocols (Qiagen,

Hilden, Germany). The total RNAs were used for cDNA synthesis using SuperScript IV reverse transcriptase (Thermo Fisher Scientific, MA, USA) with oligo dT primers, and obtained cDNAs were used for qPCR using Power SYBR Green Master Mix (Thermo Fisher Scientific, MA, USA) with gene specific primers. Primer sequences used in this study are: 5'-ATCTCTCCCGCTGAAGAGTTTTATG-3' (slc6a4a-forward), 5'-GCCAGAGGTCTTGACCCCCTTC-3' (slc6a4a-reverse), 5'-CGAGTCTAGTTCGAGTCCGC-3' (sox2-forward), 5'-CGGGCAGGTACATACTGATC-3' (sox2-rerverse), 5'-TCTGGAGGACTGTAAGAGGTATGC-3' (rpl13α-forward) [68], 5'-AGACGCACAATCTTGAGAGCA-3' (rpl13α-reverse) [68]. qPCR analysis was performed using PikoReal 96 Real-Time PCR system (Thermo Scientific, MA, USA). The expression levels of slc6a4a and sox2 relative to rpl13α were calculated by the $2^{-\Delta\Delta ct}$ method.

Microscopy and imaging

Most of individuals were observed in lateral views under a microscopy until otherwise noted. Each individual was mounted on a slide glass and adjusted for the left-light body axis to be parallel to the optical axis under a stereoscopic microscope as shown in Fig

S4. Whole body images were obtained using a stereoscopic microscope Leica MZ10F equipped with MC170 HD camera. Multicolor fluorescence images of the head and the tail were acquired using a confocal laser scanning microscope Zeiss LSM700 equipped with EC Plan-NEOFLUAR 20×/NA 0.5 and LD Plan-NEOFLUAR 40×/NA 0.6 objectives. The acquisition and the analysis of images were performed after validating our methods using different transgenic lines. To avoid the variance of fluorescence intensity by image-acquiring conditions, the conditions were initially determined using the control individuals per experiment, and all images were acquired under the same conditions. Each confocal image was obtained by compiling approximately 30–40 optical sections at 2.0 μm intervals per hemisphere using a sequential-scanning mode per each frame with 512 × 512 frame size and 8-bit depth. As a control, the mode of the fluorescence intensity frequency distribution within the ROI set in the hindbrain (see S4 Fig, B, C), which was 20, was regarded as the background level and removed from the compiled images. The same image processing was applied to all the images obtained by each experiment.

Social behavioral analysis

A test case (68 mm length × 39 mm width × 15 mm height) divided into three

compartments (sibling, no sibling areas, 10-mm length on both sides; test area, 38-mm length in the center) was used to observe social behaviors of young fish (35–37 dpf). Swimming behaviors in the test case were recorded by capturing movies using a cMOS camera (Blackfly S BFS-U3-32S4M, Point Grey) for 5 min at 50 frames per sec (fps). Each experiment was performed in order of five steps as follows: (1) A fish was transferred to the test area and habituated for 5 min. (2) Without siblings, swimming behavior was recorded for 5 min (no sibling trial). (3) Siblings were transferred to the sibling area and habituated for 5min. (4) With siblings, swimming behavior was recorded for 5 min (sibling trial). (5) Captured movies were converted to avi format using ImageJ software, and tracking analysis of the swimming fish was performed using UMATracker software (Release 15). Social behaviors were analyzed by comparing (2) with (4) for Social Preference Index (SPI) calculated as follows: SPI = (Sibling frames – No sibling frames) / Total frames [50]. Sibling frames (blue) were defined as fish located in a half region on the side of sibling area, while no sibling frames (red) were defined as fish located in the other region in the test area. A value of SPI varied between –1 and 1 [50]. SPI difference is positive when SPI in the sibling trial is larger than the no sibling trial, and negative when SPI in the sibling trial is smaller than the no sibling trial. Difference in total distance was defined as the value in sibling trial subtracting that

in no sibling trial.

Quantification and statistical analysis

Body length, head area and Kaede, GFP or mCherry-positive areas and intensities were measured using Adobe Photoshop (2023, Ver. 24.4.1) and ImageJ (Ver. 1.53). Confocal stacks were converted into 2D images using sum intensity projection. To eliminate ectopic signals derived from noise, regions exceeding a defined threshold and comprising contiguous pixels with an area of 3 pixels or more were considered as foreground. The regions were defined as the fluorescence-positive area, and the area and fluorescence mean intensity were measured. An average of control values was calculated, and then each value of individuals was represented as a relative value to the average. Thus, the average of controls was denoted as 1.0 for every experiment. For statistical analysis of two or more samples, two-tailed, unpaired nonparametric Mann-Whitney U test or Kruskal-Wallis with Dunn's multiple comparison tests were performed, unless otherwise noted, using GraphPad Prism 9 (Ver. 9.5.1).

Acknowledgements

We are grateful to Hiroshi Handa, Keisuke Miyazawa, Masaki Hiramoto (Tokyo Medical University) for valuable discussions and generous support. We thank members of Department of Anatomy and Experimental Animals (Saitama Medical University) and Hiromi Kazama (Tokyo Medical University) for help and technical support. Tg(*elavl3:Kaede*), Tg(*pou4f1-hsp70l:GFP*), Tg(*gfap:Gal4FF;UAS:GFP*) and SAGFF120A were provided from Zebrafish National BioResource Project. Tg(*pou4f3:GAL4;UAS:mCherry*) were provided by Herwig Baier. This work was supported by JSPS KAKENHI Grant Numbers 18K09271 to T.S. and T.Ka., 22K09625 to T.S., S.T., T.Ku. and T. Ka., Saitama Medical University support grant for collaboration with Saitama University 21-J-04 to T.S. and S.T., 23-J-03 to T.S., S.T. and T.Ka., Research Grant from Saitama Medical University 27-B-1-29 to T.S., and NIBB Collaborative Research Program (24NIBB528) to T.S. This work was also supported by JSPS KAKENHI Grant Number JP22H04926, Grant-in-Aid for Transformative Research Areas — Platforms for Advanced Technologies and Research Resources “Advanced Bioimaging Support”.

Author contributions

T.S. conceived and designed the experiments. T.S., T.Ku. performed the anatomy and pharmacology experiments, and K.S., T.O. performed behavioral experiments. T.S., K.S., S.T. analyzed the data. T.S., S.T., T.Ka., and M.N. wrote and edited the manuscript.

Competing interests

The authors declare no competing interests.

References

1. Sestan N, State MW. Lost in Translation: Traversing the Complex Path from Genomics to Therapeutics in Autism Spectrum Disorder. Neuron. 2018;100(2):406-23. doi: 10.1016/j.neuron.2018.10.015.

2. Amaral DG, Schumann CM, Nordahl CW. Neuroanatomy of autism. Trends Neurosci. 2008;31(3):137-45. doi: 10.1016/j.tins.2007.12.005.

3. Iakoucheva LM, Muotri AR, Sebat J. Getting to the Cores of Autism. Cell. 2019;178(6):1287-98. doi: 10.1016/j.cell.2019.07.037.

4. Willsey HR, Willsey AJ, Wang B, State MW. Genomics, convergent neuroscience and progress in understanding autism spectrum disorder. Nat Rev Neurosci. 2022;23(6):323-41. doi: 10.1038/s41583-022-00576-7.

5. Al-Haddad BJS, Oler E, Armistead B, Elsayed NA, Weinberger DR, Bernier R, et al. The fetal origins of mental illness. Am J Obstet Gynecol. 2019;221(6):549-62. doi: 10.1016/j.ajog.2019.06.013.

6. Amgalan A, Andescavage N, Limperopoulos C. Prenatal origins of neuropsychiatric diseases. Acta Paediatr. 2021;110(6):1741-9. doi: 10.1111/apa.15766.

7. Wiggins LD, Rubenstein E, Daniels J, DiGuiseppi C, Yeargin-Allsopp M, Schieve LA, et al. A Phenotype of Childhood Autism Is Associated with Preexisting Maternal Anxiety and Depression. J Abnorm Child Psychol. 2019;47(4):731-40. doi: 10.1007/s10802-018-0469-8.

8. Howard LM, Molyneaux E, Dennis CL, Rochat T, Stein A, Milgrom J.

Non-psychotic mental disorders in the perinatal period. Lancet. 2014;384(9956):1775-88. doi: 10.1016/S0140-6736(14)61276-9.

9. Hendrick V, Stowe ZN, Altshuler LL, Hwang S, Lee E, Haynes D. Placental passage of antidepressant medications. Am J Psychiatry. 2003;160(5):993-6. doi: 10.1176/appi.ajp.160.5.993.

10. Ewing G, Tatarchuk Y, Appleby D, Schwartz N, Kim D. Placental transfer of antidepressant medications: implications for postnatal adaptation syndrome. Clin Pharmacokinet. 2015;54(4):359-70. doi: 10.1007/s40262-014-0233-3.

11. Croen LA, Grether JK, Yoshida CK, Odouli R, Hendrick V. Antidepressant use during pregnancy and childhood autism spectrum disorders. Arch Gen Psychiatry. 2011;68(11):1104-12. doi: 10.1001/archgenpsychiatry.2011.73.

12. Velasquez JC, Goeden N, Bonnin A. Placental serotonin: implications for the developmental effects of SSRIs and maternal depression. Front Cell Neurosci. 2013;7:47. doi: 10.3389/fncel.2013.00047.

13. Millard SJ, Weston-Green K, Newell KA. The effects of maternal antidepressant use on offspring behaviour and brain development: Implications for risk of neurodevelopmental disorders. Neurosci Biobehav Rev. 2017;80:743-65. doi: 10.1016/j.neubiorev.2017.06.008.

14. Andalib S, Emamhadi MR, Yousefzadeh-Chabok S, Shakouri SK, Hoilund-Carlsen PF, Vafaee MS, et al. Maternal SSRI exposure increases the risk of autistic offspring: A meta-analysis and systematic review. Eur Psychiatry. 2017;45:161-6. doi: 10.1016/j.eurpsy.2017.06.001.

15. Nardozza LM, Caetano AC, Zamarian AC, Mazzola JB, Silva CP, Marcal VM, et al. Fetal growth restriction: current knowledge. Arch Gynecol Obstet. 2017;295(5):1061-77. doi: 10.1007/s00404-017-4341-9.

16. Dall'Asta A, Brunelli V, Prefumo F, Frusca T, Lees CC. Early onset fetal growth restriction. Matern Health Neonatol Perinatol. 2017;3:2. doi: 10.1186/s40748-016-0041-x.

17. Pels A, Knaven OC, Wijnberg-Williams BJ, Eijsermans MJC, Mulder-de Tollenaer SM, Aarnoudse-Moens CSH, et al. Neurodevelopmental outcomes at five years after early-onset fetal growth restriction: Analyses in a Dutch subgroup participating in a European management trial. Eur J Obstet Gynecol Reprod Biol. 2019;234:63-70. doi: 10.1016/j.ejogrb.2018.12.041.

18. Ranzil S, Ellery S, Walker DW, Vaillancourt C, Alfaidy N, Bonnin A, et al. Disrupted placental serotonin synthetic pathway and increased placental serotonin: Potential implications in the pathogenesis of human fetal growth restriction.

Placenta. 2019;84:74-83. doi: 10.1016/j.placenta.2019.05.012.

19. Joseph RM, Korzeniewski SJ, Allred EN, O'Shea TM, Heeren T, Frazier JA, et al. Extremely low gestational age and very low birthweight for gestational age are risk factors for autism spectrum disorder in a large cohort study of 10-year-old children born at 23-27 weeks' gestation. Am J Obstet Gynecol. 2017;216(3):304 e1- e16. doi: 10.1016/j.ajog.2016.11.1009.

20. Gaspar P, Cases O, Maroteaux L. The developmental role of serotonin: news from mouse molecular genetics. Nat Rev Neurosci. 2003;4(12):1002-12. doi: 10.1038/nrn1256.

21. Pourhamzeh M, Moravej FG, Arabi M, Shahriari E, Mehrabi S, Ward R, et al. The Roles of Serotonin in Neuropsychiatric Disorders. Cell Mol Neurobiol. 2022;42(6):1671-92. doi: 10.1007/s10571-021-01064-9.

22. Otte C, Gold SM, Penninx BW, Pariante CM, Etkin A, Fava M, et al. Major depressive disorder. Nat Rev Dis Primers. 2016;2:16065. doi: 10.1038/nrdp.2016.65.

23. Gross C, Zhuang X, Stark K, Ramboz S, Oosting R, Kirby L, et al. Serotonin1A receptor acts during development to establish normal anxiety-like behaviour in the adult. Nature. 2002;416(6879):396-400. doi: 10.1038/416396a.

24. Aimone JB, Li Y, Lee SW, Clemenson GD, Deng W, Gage FH. Regulation and function of adult neurogenesis: from genes to cognition. Physiol Rev. 2014;94(4):991-1026. doi: 10.1152/physrev.00004.2014.

25. Bonnin A, Goeden N, Chen K, Wilson ML, King J, Shih JC, et al. A transient placental source of serotonin for the fetal forebrain. Nature. 2011;472(7343):347-50. doi: 10.1038/nature09972.

26. Rosenfeld CS. The placenta-brain-axis. J Neurosci Res. 2021;99(1):271-83. doi: 10.1002/jnr.24603.

27. St-Pierre J, Laurent L, King S, Vaillancourt C. Effects of prenatal maternal stress on serotonin and fetal development. Placenta. 2016;48 Suppl 1:S66-S71. doi: 10.1016/j.placenta.2015.11.013.

28. Trowbridge S, Narboux-Neme N, Gaspar P. Genetic models of serotonin (5-HT) depletion: what do they tell us about the developmental role of 5-HT? Anat Rec (Hoboken). 2011;294(10):1615-23. doi: 10.1002/ar.21248.

29. Rea V, Van Raay TJ. Using Zebrafish to Model Autism Spectrum Disorder: A Comparison of ASD Risk Genes Between Zebrafish and Their Mammalian Counterparts. Front Mol Neurosci. 2020;13:575575. doi: 10.3389/fnmol.2020.575575.

30. Sakai C, Ijaz S, Hoffman EJ. Zebrafish Models of Neurodevelopmental Disorders: Past, Present, and Future. Front Mol Neurosci. 2018;11:294. doi: 10.3389/fnmol.2018.00294.

31. Sato T, Sato F, Kamezaki A, Sakaguchi K, Tanigome R, Kawakami K, et al. Neuregulin 1 Type II-ErbB Signaling Promotes Cell Divisions Generating Neurons from Neural Progenitor Cells in the Developing Zebrafish Brain. PLoS One. 2015;10(5):e0127360. doi: 10.1371/journal.pone.0127360.

32. Bourin M, Chue P, Guillon Y. Paroxetine: a review. CNS Drug Rev. 2001;7(1):25-47. doi: 10.1111/j.1527-3458.2001.tb00189.x.

33. Coleman JA, Green EM, Gouaux E. X-ray structures and mechanism of the human serotonin transporter. Nature. 2016;532(7599):334-9. doi: 10.1038/nature17629.

34. Coleman JA, Navratna V, Antermite D, Yang D, Bull JA, Gouaux E. Chemical and structural investigation of the paroxetine-human serotonin transporter complex. Elife. 2020;9. doi: 10.7554/eLife.56427.

35. Lillesaar C, Stigloher C, Tannhauser B, Wullimann MF, Bally-Cuif L. Axonal projections originating from raphe serotonergic neurons in the developing and adult zebrafish, Danio rerio, using transgenics to visualize raphe-specific pet1 expression. J Comp Neurol. 2009;512(2):158-82. doi: 10.1002/cne.21887.

36. Ito T, Handa H. Deciphering the mystery of thalidomide teratogenicity. Congenit Anom (Kyoto). 2012;52(1):1-7. doi: 10.1111/j.1741-4520.2011.00351.x.

37. Chen X, Liu H, Li Y, Zhang W, Zhou A, Xia W, et al. First-trimester fetal size, accelerated growth in utero, and child neurodevelopment in a cohort study. BMC Med. 2024;22(1):181. doi: 10.1186/s12916-024-03390-3.

38. Niell CM, Meyer MP, Smith SJ. In vivo imaging of synapse formation on a growing dendritic arbor. Nat Neurosci. 2004;7(3):254-60. doi: 10.1038/nn1191.

39. Hua JY, Smear MC, Baier H, Smith SJ. Regulation of axon growth in vivo by activity-based competition. Nature. 2005;434(7036):1022-6. doi: 10.1038/nature03409.

40. Sato T, Hamaoka T, Aizawa H, Hosoya T, Okamoto H. Genetic single-cell mosaic analysis implicates ephrinB2 reverse signaling in projections from the posterior tectum to the hindbrain in zebrafish. J Neurosci. 2007;27(20):5271-9. doi: 10.1523/JNEUROSCI.0883-07.2007.

41. Isa T, Marquez-Legorreta E, Grillner S, Scott EK. The tectum/superior colliculus as the vertebrate solution for spatial sensory integration and action. Curr Biol. 2021;31(11):R741-R62. Epub 2021/06/09. doi: 10.1016/j.cub.2021.04.001.

42. Xiao T, Baier H. Lamina-specific axonal projections in the zebrafish tectum require

the type IV collagen Dragnet. Nat Neurosci. 2007;10(12):1529-37. Epub 2007/11/06. doi: 10.1038/nn2002.

43. Obholzer N, Wolfson S, Trapani JG, Mo W, Nechiporuk A, Busch-Nentwich E, et al. Vesicular glutamate transporter 3 is required for synaptic transmission in zebrafish hair cells. J Neurosci. 2008;28(9):2110-8. doi: 10.1523/JNEUROSCI.5230-07.2008.

44. Sato T, Takahoko M, Okamoto H. HuC:Kaede, a useful tool to label neural morphologies in networks in vivo. Genesis. 2006;44(3):136-42. doi: 10.1002/gene.20196.

45. Boldrini M, Hen R, Underwood MD, Rosoklija GB, Dwork AJ, Mann JJ, et al. Hippocampal angiogenesis and progenitor cell proliferation are increased with antidepressant use in major depression. Biol Psychiatry. 2012;72(7):562-71. doi: 10.1016/j.biopsych.2012.04.024.

46. Greig LC, Woodworth MB, Galazo MJ, Padmanabhan H, Macklis JD. Molecular logic of neocortical projection neuron specification, development and diversity. Nat Rev Neurosci. 2013;14(11):755-69. doi: 10.1038/nrn3586.

47. Ando H, Sato T, Ito T, Yamamoto J, Sakamoto S, Nitta N, et al. Cereblon Control of Zebrafish Brain Size by Regulation of Neural Stem Cell Proliferation. iScience.

2019;15:95-108. doi: 10.1016/j.isci.2019.04.007.

48. Scott EK, Mason L, Arrenberg AB, Ziv L, Gosse NJ, Xiao T, et al. Targeting neural circuitry in zebrafish using GAL4 enhancer trapping. Nat Methods. 2007;4(4):323-6. doi: 10.1038/nmeth1033.

49. Lal P, Tanabe H, Suster ML, Ailani D, Kotani Y, Muto A, et al. Identification of a neuronal population in the telencephalon essential for fear conditioning in zebrafish. BMC Biol. 2018;16(1):45. doi: 10.1186/s12915-018-0502-y.

50. Dreosti E, Lopes G, Kampff AR, Wilson SW. Development of social behavior in young zebrafish. Front Neural Circuits. 2015;9:39. doi: 10.3389/fncir.2015.00039.

51. Levkovitz Y, Gil-Ad I, Zeldich E, Dayag M, Weizman A. Differential induction of apoptosis by antidepressants in glioma and neuroblastoma cell lines: evidence for p-c-Jun, cytochrome c, and caspase-3 involvement. J Mol Neurosci. 2005;27(1):29-42. doi: 10.1385/JMN:27:1:029.

52. Schuster C, Fernbach N, Rix U, Superti-Furga G, Holy M, Freissmuth M, et al. Selective serotonin reuptake inhibitors--a new modality for the treatment of lymphoma/leukaemia? Biochem Pharmacol. 2007;74(9):1424-35. doi: 10.1016/j.bcp.2007.07.017.

53. Wei P, Jia H, Li R, Zhang C, Guo S, Wei S, et al. Fluvoxamine prompts the

antitumor immune effect via inhibiting the PD-L1 expression on mice-burdened colon tumor. Cell Biol Int. 2023;47(2):439-50. doi: 10.1002/cbin.11936.

54. Hodge JM, Wang Y, Berk M, Collier FM, Fernandes TJ, Constable MJ, et al. Selective serotonin reuptake inhibitors inhibit human osteoclast and osteoblast formation and function. Biol Psychiatry. 2013;74(1):32-9. doi: 10.1016/j.biopsych.2012.11.003.

55. Reis G, Dos Santos Moreira-Silva EA, Silva DCM, Thabane L, Milagres AC, Ferreira TS, et al. Effect of early treatment with fluvoxamine on risk of emergency care and hospitalisation among patients with COVID-19: the TOGETHER randomised, platform clinical trial. Lancet Glob Health. 2022;10(1):e42-e51. doi: 10.1016/S2214-109X(21)00448-4.

56. Hashimoto Y, Suzuki T, Hashimoto K. Mechanisms of action of fluvoxamine for COVID-19: a historical review. Mol Psychiatry. 2022;27(4):1898-907. doi: 10.1038/s41380-021-01432-3.

57. Asatsuma-Okumura T, Ando H, De Simone M, Yamamoto J, Sato T, Shimizu N, et al. p63 is a cereblon substrate involved in thalidomide teratogenicity. Nat Chem Biol. 2019;15(11):1077-84. doi: 10.1038/s41589-019-0366-7.

58. Miller MT, Stromland K, Ventura L, Johansson M, Bandim JM, Gillberg C. Autism

with ophthalmologic malformations: the plot thickens. Trans Am Ophthalmol Soc. 2004;102:107-20; discussion 20-1.

59. Sato T, Ito T, Handa H. Cereblon-Based Small-Molecule Compounds to Control Neural Stem Cell Proliferation in Regenerative Medicine. Front Cell Dev Biol. 2021;9:629326. doi: 10.3389/fcell.2021.629326.

60. Ito T, Yamaguchi Y, Handa H. Exploiting ubiquitin ligase cereblon as a target for small-molecule compounds in medicine and chemical biology. Cell Chem Biol. 2021;28(7):987-99. doi: 10.1016/j.chembiol.2021.04.012.

61. Kriegstein A, Alvarez-Buylla A. The glial nature of embryonic and adult neural stem cells. Annu Rev Neurosci. 2009;32:149-84. doi: 10.1146/annurev.neuro.051508.135600.

62. Suh H, Consiglio A, Ray J, Sawai T, D'Amour KA, Gage FH. In vivo fate analysis reveals the multipotent and self-renewal capacities of Sox2+ neural stem cells in the adult hippocampus. Cell Stem Cell. 2007;1(5):515-28. doi: 10.1016/j.stem.2007.09.002.

63. Sahay A, Hen R. Adult hippocampal neurogenesis in depression. Nat Neurosci. 2007;10(9):1110-5. doi: 10.1038/nn1969.

64. Persico AM, Baldi A, Dell'Acqua ML, Moessner R, Murphy DL, Lesch KP, et al.

Reduced programmed cell death in brains of serotonin transporter knockout mice. Neuroreport. 2003;14(3):341-4. doi: 10.1097/00001756-200303030-00009.

65. Salichon N, Gaspar P, Upton AL, Picaud S, Hanoun N, Hamon M, et al. Excessive activation of serotonin (5-HT) 1B receptors disrupts the formation of sensory maps in monoamine oxidase a and 5-ht transporter knock-out mice. J Neurosci. 2001;21(3):884-96. doi: 10.1523/JNEUROSCI.21-03-00884.2001.

66. Upton AL, Ravary A, Salichon N, Moessner R, Lesch KP, Hen R, et al. Lack of 5-HT(1B) receptor and of serotonin transporter have different effects on the segregation of retinal axons in the lateral geniculate nucleus compared to the superior colliculus. Neuroscience. 2002;111(3):597-610. doi: 10.1016/s0306-4522(01)00602-9.

67. Avino TA, Barger N, Vargas MV, Carlson EL, Amaral DG, Bauman MD, et al. Neuron numbers increase in the human amygdala from birth to adulthood, but not in autism. Proc Natl Acad Sci U S A. 2018;115(14):3710-5. doi: 10.1073/pnas.1801912115.

68. Westerfield M. THE ZEBRAFISH BOOK, 5th ed. A guide for the laboratory use of zebrafish (Danio rerio). Eugene: University of Oregon Press; 2007.

69. Waugh TA, Horstick E, Hur J, Jackson SW, Davidson AE, Li X, et al. Fluoxetine

prevents dystrophic changes in a zebrafish model of Duchenne muscular dystrophy. Hum Mol Genet. 2014;23(17):4651-62. doi: 10.1093/hmg/ddu185.

70. Rassier GT, Silveira TLR, Remiao MH, Daneluz LO, Martins AWS, Dellagostin EN, et al. Evaluation of qPCR reference genes in GH-overexpressing transgenic zebrafish (Danio rerio). Sci Rep. 2020;10(1):12692. doi: 10.1038/s41598-020-69423-y.

Supporting information

S1 Fig. Distribution and knockdown of zebrafish SLC6A4a. (**A**) Immunostaining with anti-SERT antibody for 30-hpf SLC6A4a-knockdown (KD) embryos by injection of slc6a4a antisense MO (AMO) and the control (5mis). (**B**) Quantification of immunofluorescent signals in SLC6A4a-KD embryos. (**C**) Expression of *slc6a4a* mRNAs in SLC6A4a-KD embryos by RT-qPCR. (**D**) Lateral views of 32-hpf embryos injected with antisense slc6a4a-AMO and the control slc6a4a-5mis. White line, head-tail body length. (**E**, **F**) Quantification of the body length (**E**) and the head area (**F**) of the injected embryos. (**G**) Lateral views of 32-hpf Tg(*elavl3:Kaede*) embryos

injected with MOs (top) and those embryos immunostained for active Caspase-3 (bottom). (**H**) Quantification of the intensity of active Caspase-3 signals in the brain of the injected embryos. Scale bars: 200 μm (**D**); 100 μm (**A**, **G**). Data are presented as mean ± SEM. *$p < 0.05$, ***$p < 0.001$, Mann-Whitney U test.

S2 Fig. Development of morphology and the retinotectal projection in wild-type embryos. (**A**) Lateral views of wild-type embryos at 50 hpf, 72 hpf, 5 dpf, and 7 dpf. White line, head-tail body length. (**B**, **C**) Quantification of the body length (**B**) and the head area (**C**) of wild-type embryos. (**D**) Lateral views of wild-type Tg(*pou4f1-hsp70l:GFP;pau4f3:GAL4;UAS:mCherry*) embryos at 72 hpf, 5 dpf, 7 dpf. GFP (green) expressed in tectal neurons and retinal axons. mCherry (red) expressed in retinal axons. (**E**, **F**) Quantification of GFP-positive (**E**) and mCherry-positive (**F**) areas in the optic tectum. (**G**, **H**) Quantification of the intensity of GFP (**G**) and mCherry (**H**) in the optic tectum. Scale bars: 200 μm (**A**); 100 μm (**D**). Data are presented as mean ± SEM. *$p < 0.05$, **$p < 0.01$, ***$p < 0.001$, ****$p < 0.0001$, ns, not significant. Kruskal-Wallis with Dunn's multiple comparisons tests.

S3 Fig. Effects of early paroxetine on embryogenesis and neurogenesis at 3 dpf. (**A**) A schematic diagram of treatment with 1 μM paroxetine. (**B**) Lateral views of 73-hpf embryos treated with paroxetine and the control DMSO. (**C**, **D**) Quantification of the body length (**C**) and the head area (**D**) of the treated embryos. (**E**) A schematic diagram of treatment with 10 μM paroxetine. (**F**) Lateral views of 72-hpf embryos treated with paroxetine and the control DMSO. (**G**, **H**) Quantification of the body length (**G**) and the head area (**H**) of the treated embryos. (**I**) Lateral views of 72-hpf Tg(*pou4f1-hsp70l:GFP*) embryos treated with 10 μM paroxetine and the control DMSO. (**J**) Quantification of GFP intensity in the optic tectum of the treated embryos. White lines, head-tail body length. Parox, paroxetine. Scale bars: 200 μm (**B**, **F**); 100 μm (**I**). Data are presented as mean ± SEM. *$p < 0.05$, **$p < 0.01$, ***$p < 0.001$, ****$p < 0.0001$, Mann-Whitney U test.

S4 Fig. Effects of early paroxetine on neurogenesis. (**A**) Lateral views of a 50-hpf Tg(*neurod:EGFP*) embryo. Regions and lines for quantification of the intensity are indicated in the bottom image. (**B**) Intensity profiles of the yellow arrows in (**A**, bottom) in the optic tectum (green dots) and the hindbrain (gray dots). (**C**) Intensity frequencies of the regions (white squares in **A**, bottom) in the optic tectum (green dots) and the

hindbrain (gray dots). (**D**) A schematic for the time course of treatment with paroxetine. (**E**) Lateral views of 50-hpf Tg(*elavl3:Kaede*) embryos treated with 1 μM, 10 μM paroxetine and the control DMSO. (**F**–**I**) Quantification of Kaede-positive area (**F**, **G**) and the intensity (**G**, **I**) in the optic tectum (**F**, **G**) and the telencephalon (**H**, **I**) of 10 μM paroxetine-treated embryos. (**J**) Lateral views of DMSO- and paroxetine-treated embryos immunostained for SOX2 (red). (**K**, **L**) Quantification of the expression of SOX2 protein by immunohistochemistry (**H**), and *sox2* mRNA by RT-qPCR (**I**). Parox, paroxetine. Cb, cerebellum; e, eye; H, hindbrain; OT, optic tectum; T, telencephlon. Filled arrowhead, optic tectum; open arrowhead, telencephalon. Scale bars, 100 μm. Data are presented as mean ± SEM. *$p < 0.05$, **$p < 0.01$, Mann-Whitney U test.

S5 Fig. Growth restriction and suppressed neurogenesis by early transient paroxetine at 5 dpf. (**A**) A schematic diagram of treatment with 10 μM paroxetine and 5-HT. (**B**) Lateral views of 5-dpf larvae treated with paroxetine, 5-HT and the control DMSO. White line, head-tail body length. (**C**, **D**) Quantification of the body length (**C**) and the head area (**D**) of the treated larvae. (**E**) Lateral views of 5-dpf Tg(*pou4f1-hsp70l:GFP*) larvae treated with 10 μM paroxetine and the control DMSO. (**F**, **G**) Quantification of GFP-positive area (**E**) and the intensity (**F**) in the optic tectum

of the treated larvae. Parox, paroxetine. Scale bars: 200 μm (**B)**; 100 μm (**E**). Data are mean ± SEM. *$p < 0.05$, ***$p < 0.001$, ns, not significant. Kruskal-Wallis with Dunn's multiple comparisons tests (**C**, **D**), Mann-Whitney U test (**F**, **G**).

S6 Fig. Suppressed neurogenesis in the dorsal telencephalon and restored head morphology in paroxetine and 5-HT-treated 7-dpf larvae. a A schematic diagram of treatment with 1 μM paroxetine. **b**, **c** Quantification of GFP intensity in the dorsal telencephalon of the paroxetine-treated larvae (**b**), and 5-HT-treated larvae (**c**). **d, e** Dorsal views of 76-hpf SAGFF120A;UAS:GFP larvae treated with paroxetine, and the control DMSO (**d**), 5-HT and the control (**e**). **f** A schematic diagram of treatment with 1 μM paroxetine and 5-HT. **g** Lateral views of 7-dpf larvae treated with paroxetine, 5-HT and the control DMSO. White line, head-tail body length. **h**, **i** Quantification of the body length (**h**) and the head area (**i**) of the treated larvae. Parox, paroxetine. Scale bars: 100 μm (**b**); 200 μm (**e**). Data are mean ± SEM. *$p < 0.05$, **$p < 0.01$, ***$p < 0.001$, ns, not significant. Mann-Whitney U test (**b**, **c**), Kruskal-Wallis with Dunn's multiple comparisons tests (**h**, **i**).

S1 Video. DMSO-treated fish in a no sibling trial.

S2 Video. DMSO-treated fish in a sibling trial.

S3 Video. Paroxetine-treated fish in a no sibling trial.

S4 Video. Paroxetine-treated fish in a sibling trial.

S5 Video. 5-HT-treated fish in a no sibling trial.

S6 Video. 5-HT-treated fish in a sibling trial.

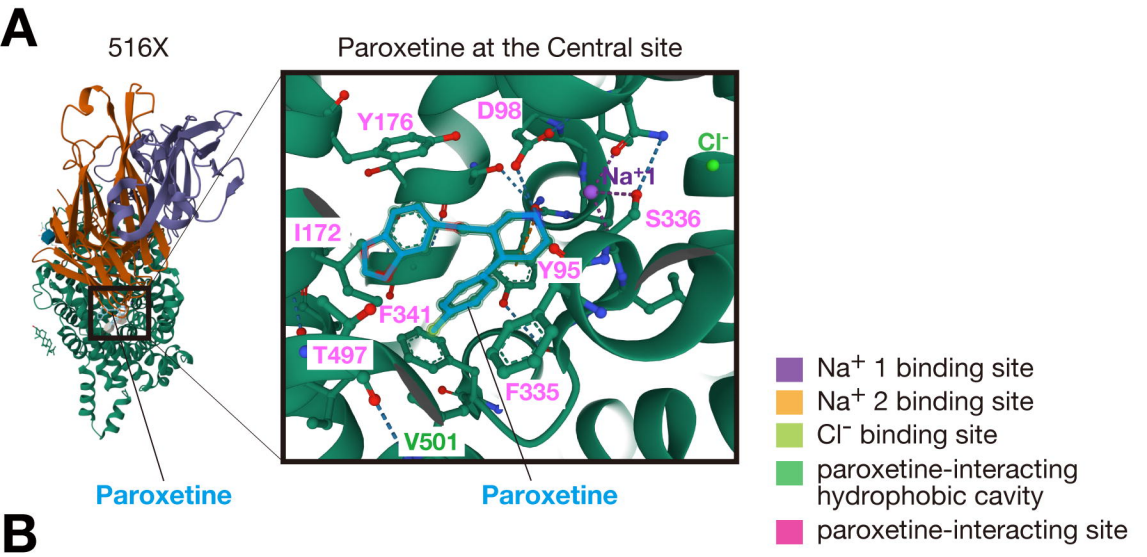

B

```
Human      1   METTPLNSQKQLSACEDGEDCQENGVLQ-KVVPTPGDKVESG--QISNGYSAV----PSP   53
           M+ + + +Q+     +   + QENG L    VP    K  SG  Q+SNGY +     P
Zebrafish  3   MKESMMMNQEYGGEQQKVPESQENGRLVVDSVPEKDQKSGSGPGQVSNGYRSTSPQSPKE   62

Human     54   GAGDDT-RHSIPATTTTLVAELHQGE--RETWGKKVDFLLSVIGYAVDLGNVWRFPYICY  110
             GAG  T R + P T  TLV +    +  RETW KK+DFLLSVIGYAVDLGNVWRFPYICY
Zebrafish 63   GAGTGTDRVNTPGTFRTLVVQQTSLDPPRETWSKKMDFLLSVIGYAVDLGNVWRFPYICY  122

Human    111   QNGGGAFLLPYTIMAIFGGIPLFYMELALGQYHRNGCISIWRKICPIFKGIGYAICIIAF  170
             QNGGGAFLLPY +MA+FGG+PLFYMELALGQ+HR+GCISIW+ +CPIFKGIG+AICIIA
Zebrafish 123  QNGGGAFLLPYLLMAVFGGVPLFYMELALGQFHRSGCISIWKHVCPIFKGIGFAICIIAL  182

Human    171   YIASYYNTIMAWALYYLISSFTDQLPWTSCKNSWNTGNCTNYFSED-NITWTLHSTSPAE  229
             YIA YYNTIMAWALYYL+SSF   LPWT+C N WNT NCT+Y S D N++WT +S SPAE
Zebrafish 183  YIAFYYNTIMAWALYYLLSSFRATLPWTTCNNRWNTPNCTHYLSTDLNVSWTNNSISPAE  242

Human    230   EFYTRHVLQIHRSKGLQDLGGISWQLALCIMLIFTVIYFSIWKGVKTSGKVVWVTATFPY  289
             EFY R VLQ+H S GL  LG +SWQLALC++ IFTV+YFSIWKGVKTSGKVVWVTATFPY
Zebrafish 243  EFYVRQVLQVHLSPGLHQLGWVSWQLALCLLFIFTVVYFSIWKGVKTSGKVVWVTATFPY  302

Human    290   IILSVLLVRGATLPGAWRGVLFYLKPNWQKLLETGVWIDAAAQIFFSLGPGFGVLLAFAS  349
             ++L +LL+RGATLPGAWRGV+FYLKP+W+KLL T VW+DAAAQIFFSLGPGFGVLLAFAS
Zebrafish 303  LVLLILLIRGATLPGAWRGVVFYLKPDWKKLLTTTVWLDAAAQIFFSLGPGFGVLLAFAS  362

Human    350   YNKFNNNCYQDALVTSVVNCMTSFVSGFVIFTVLGYMAEMRNEDVSEVAKDAGPSLLFIT  409
             YN F+NNCY+DAL+TS VNC+TSF+SGFVIFTVLGYMAEMR + V  VAKDAGPSLLFI
Zebrafish 363  YNPFHNNCYKDALITSSVNCLTSFLSGFVIFTVLGYMAEMRQQGVETVAKDAGPSLLFII  422

Human    410   YAEAIANMPASTFFAIIFFLMLITLGLDSTFAGLEGVITAVLDEFPHVWAKRRERFVLAV  469
             YAEAIANMPA+TFFAIIFFLM+I LGLDSTFAGLEGVITA+LDEFPH+ A+RRE FVL +
Zebrafish 423  YAEAIANMPAATFFAIIFFLMIIMLGLDSTFAGLEGVITAMLDEFPHLLARRREWFVLGL  482

Human    470   VITCFFGSLVTLTFGGAYVVKLLEEYATGPAVLTVALIEAVAVSWFYGITQFCRDVKEML  529
             V  C+ G+L TLT+GGA+VVKL EEYATGPAV+TV  +E +AVSWFYG T+FC DV+ ML
Zebrafish 483  VCVCYLGALSTLTYGGAFVVKLFEEYATGPAVITVVFLEVIAVSWFYGTTRFCNDVQLML  542

Human    530   GFSPGWFWRICWVAISPLFLLFIICSFLMSPPQLRLFQYNYPYWSIILGYCIGTSSFICI  589
             GF+PG FWR+CW+AI P FLLFII SFL  PP+++LF Y YP+W+ +LGYCIG SSFIC+
Zebrafish 543  GFAPGLFWRVCWIAICPCFLLFIIVSFLAFPPEVKLFDYLYPFWTTVLGYCIGVSSFICV  602

Human    590   PTYIAYRLIITPGTFKERIIKSITPETP  617
             P+Y+ Y L+ T GTF++R++K ITPE P
Zebrafish 603  PSYMVYHLVTTKGTFQQRLLKGITPEAP  630
```

C

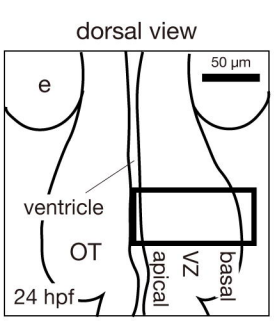

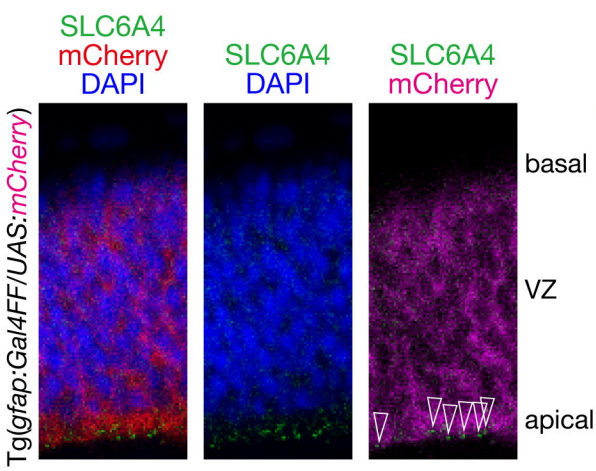

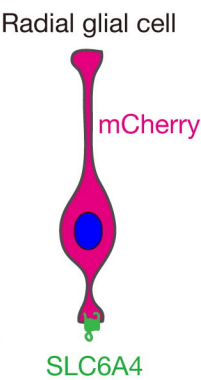

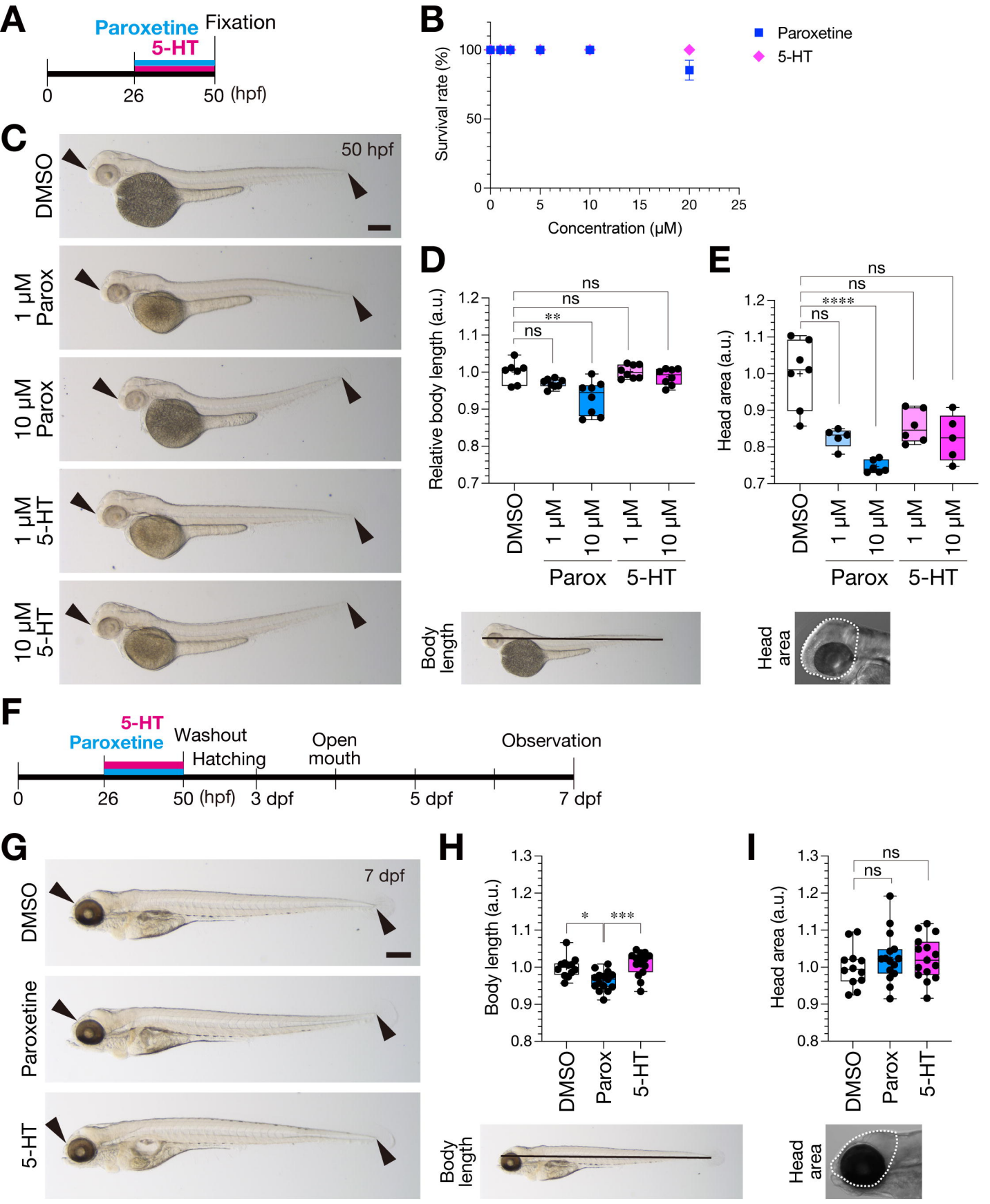
A
Paroxetine
5-HT
Fixation
0
26
50 (hpf)
B
Paroxetine
5-HT
Survival rate (%)
Concentration (μM)
C
50 hpf
DMSO
1 μM Parox
10 μM Parox
1 μM 5-HT
10 μM 5-HT
D
Relative body length (a.u.)
ns
ns
**
ns
DMSO
1 μM
10 μM
1 μM
10 μM
Parox
5-HT
Body length
E
Head area (a.u.)
ns
ns
****
ns
DMSO
1 μM
10 μM
1 μM
10 μM
Parox
5-HT
Head area
F
5-HT
Paroxetine
Washout
Hatching
Open mouth
Observation
0
26
50 (hpf)
3 dpf
5 dpf
7 dpf
G
7 dpf
DMSO
Paroxetine
5-HT
H
Body length (a.u.)
*
***
DMSO
Parox
5-HT
Body length
I
Head area (a.u.)
ns
ns
DMSO
Parox
5-HT
Head area

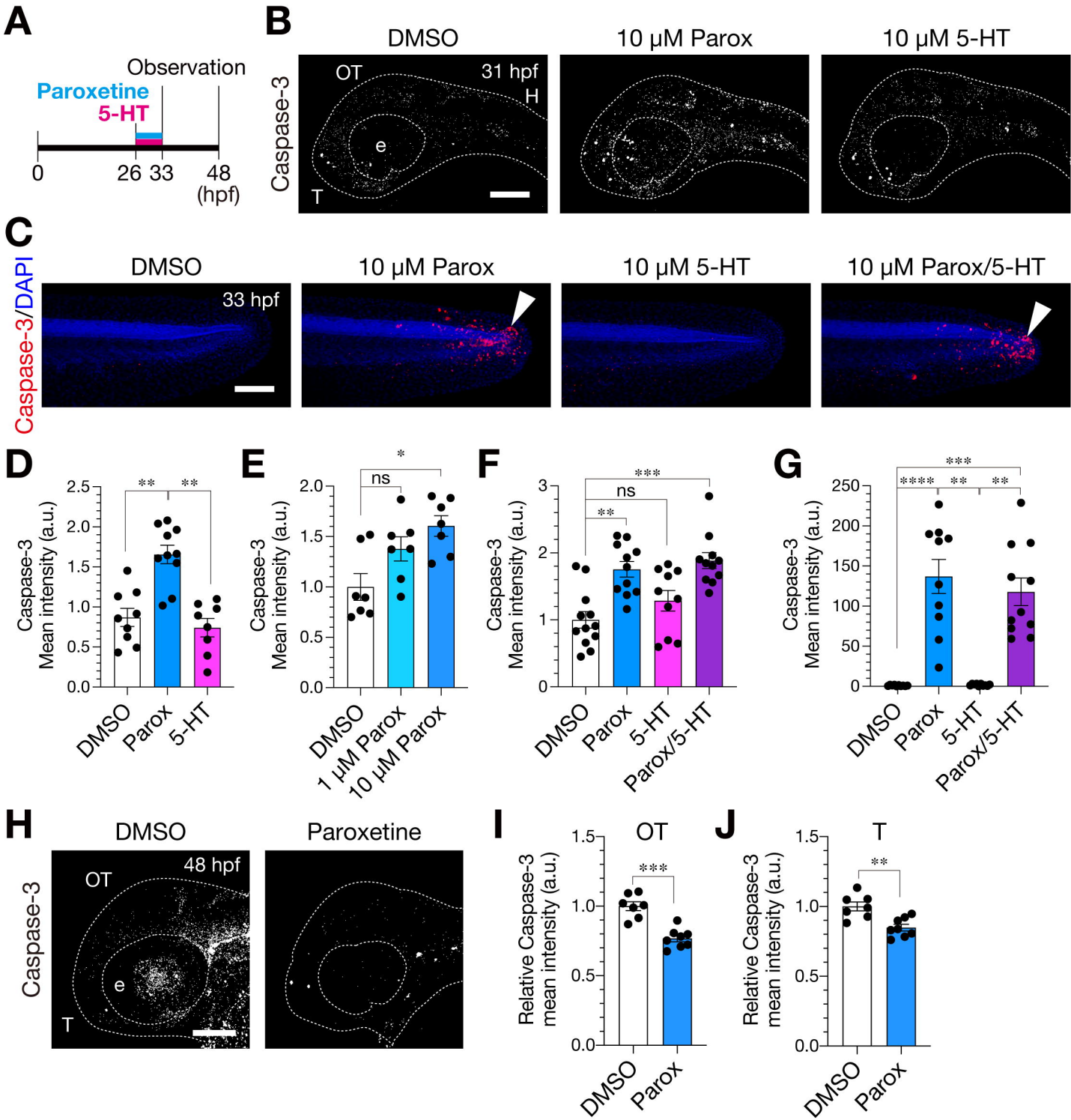
A
Observation
Paroxetine
5-HT
0
26 33
48
(hpf)
B
DMSO
10 μM Parox
10 μM 5-HT
Caspase-3
OT
31 hpf
H
e
T
C
DMSO
10 μM Parox
10 μM 5-HT
10 μM Parox/5-HT
Caspase-3/DAPI
33 hpf
D
Caspase-3
Mean intensity (a.u.)
DMSO
Parox
5-HT
E
ns
*
1 μM Parox
10 μM Parox
F
ns
**
***
Parox/5-HT
G
****
H
DMSO
Paroxetine
48 hpf
I
OT
Relative Caspase-3
mean intensity (a.u.)
J
T

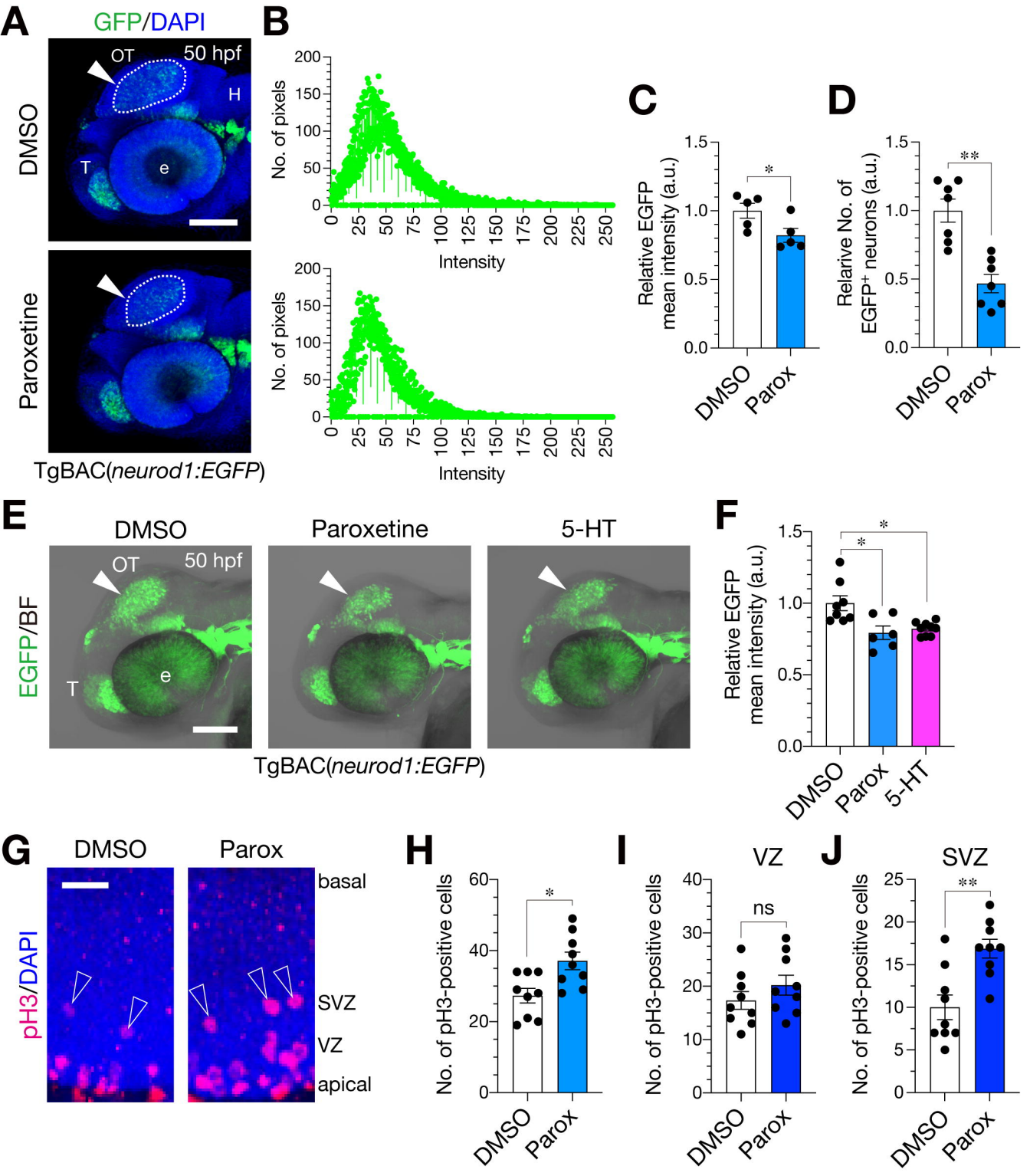
A
GFP/DAPI
50 hpf
OT
H
T
e
DMSO
Paroxetine
TgBAC(neurod1:EGFP)
B
No. of pixels
Intensity
C
Relative EGFP mean intensity (a.u.)
DMSO
Parox
D
Relarive No. of EGFP+ neurons (a.u.)
E
DMSO
Paroxetine
5-HT
EGFP/BF
F
Relative EGFP mean intensity (a.u.)
G
pH3/DAPI
basal
SVZ
VZ
apical
H
No. of pH3-positive cells
I
VZ
ns
J
SVZ

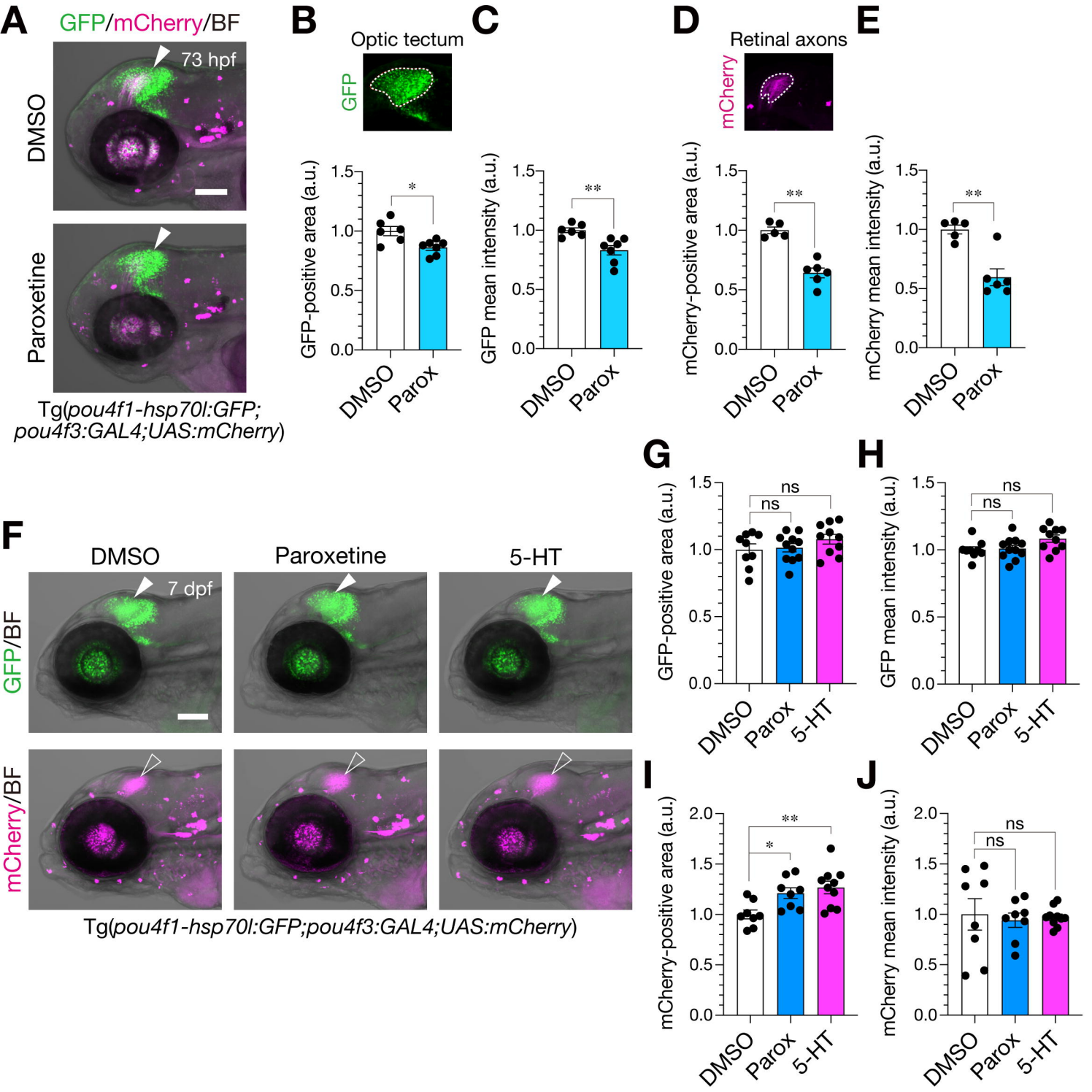
A
GFP/mCherry/BF
73 hpf
DMSO
Paroxetine
Tg(pou4f1-hsp70l:GFP; pou4f3:GAL4;UAS:mCherry)
B
Optic tectum
GFP
GFP-positive area (a.u.)
DMSO
Parox
C
GFP mean intensity (a.u.)
D
Retinal axons
mCherry
mCherry-positive area (a.u.)
E
mCherry mean intensity (a.u.)
F
DMSO
Paroxetine
5-HT
7 dpf
GFP/BF
mCherry/BF
Tg(pou4f1-hsp70l:GFP;pou4f3:GAL4;UAS:mCherry)
G
H
I
J
ns

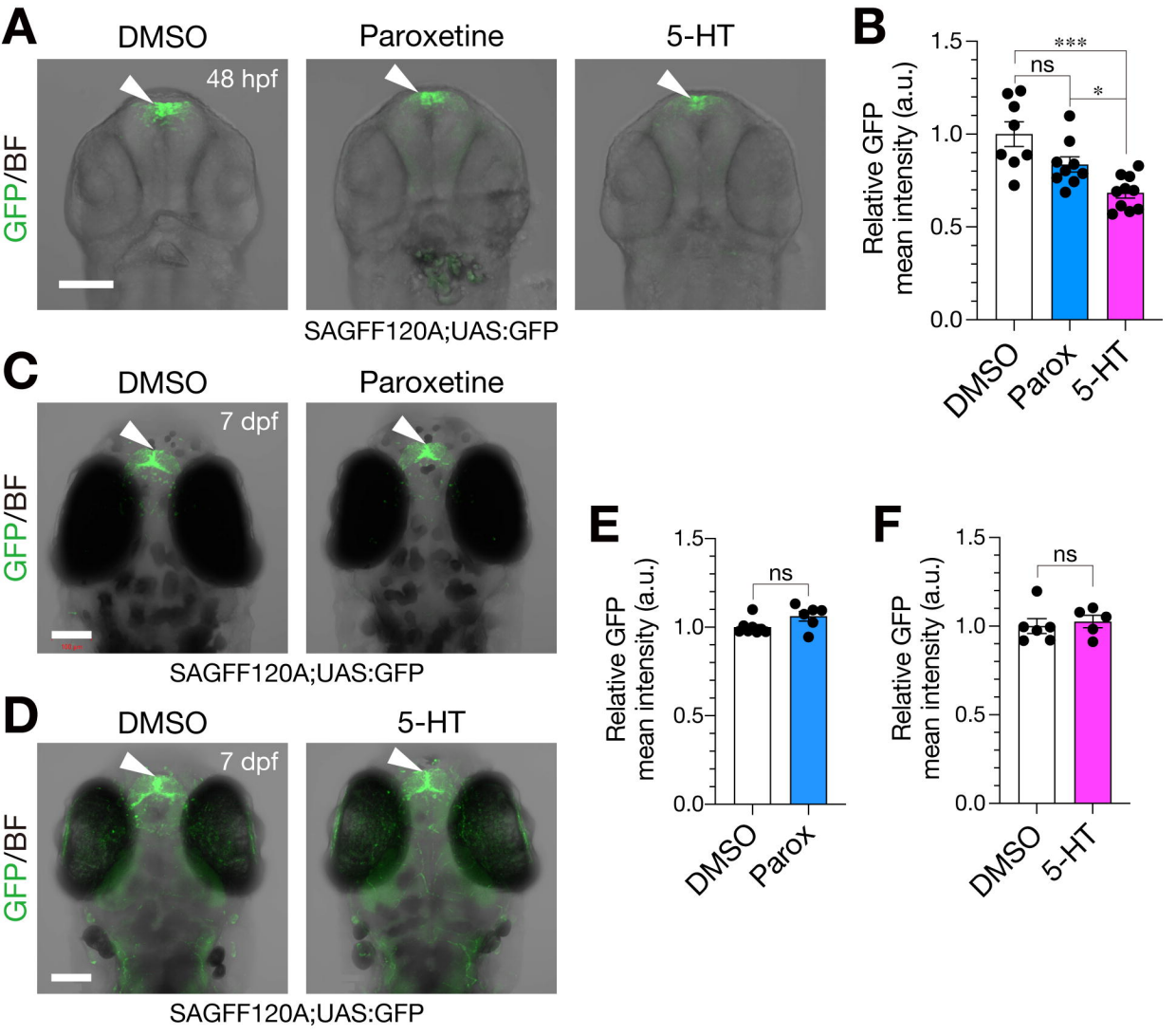
A
DMSO
Paroxetine
5-HT
48 hpf
GFP/BF
SAGFF120A;UAS:GFP
B
Relative GFP mean intensity (a.u.)
1.5
1.0
0.5
0.0
***
ns
*
DMSO
Parox
5-HT
C
DMSO
Paroxetine
7 dpf
GFP/BF
SAGFF120A;UAS:GFP
D
DMSO
5-HT
7 dpf
GFP/BF
SAGFF120A;UAS:GFP
E
Relative GFP mean intensity (a.u.)
1.5
1.0
0.5
0.0
ns
DMSO
Parox
F
Relative GFP mean intensity (a.u.)
1.5
1.0
0.5
0.0
ns
DMSO
5-HT

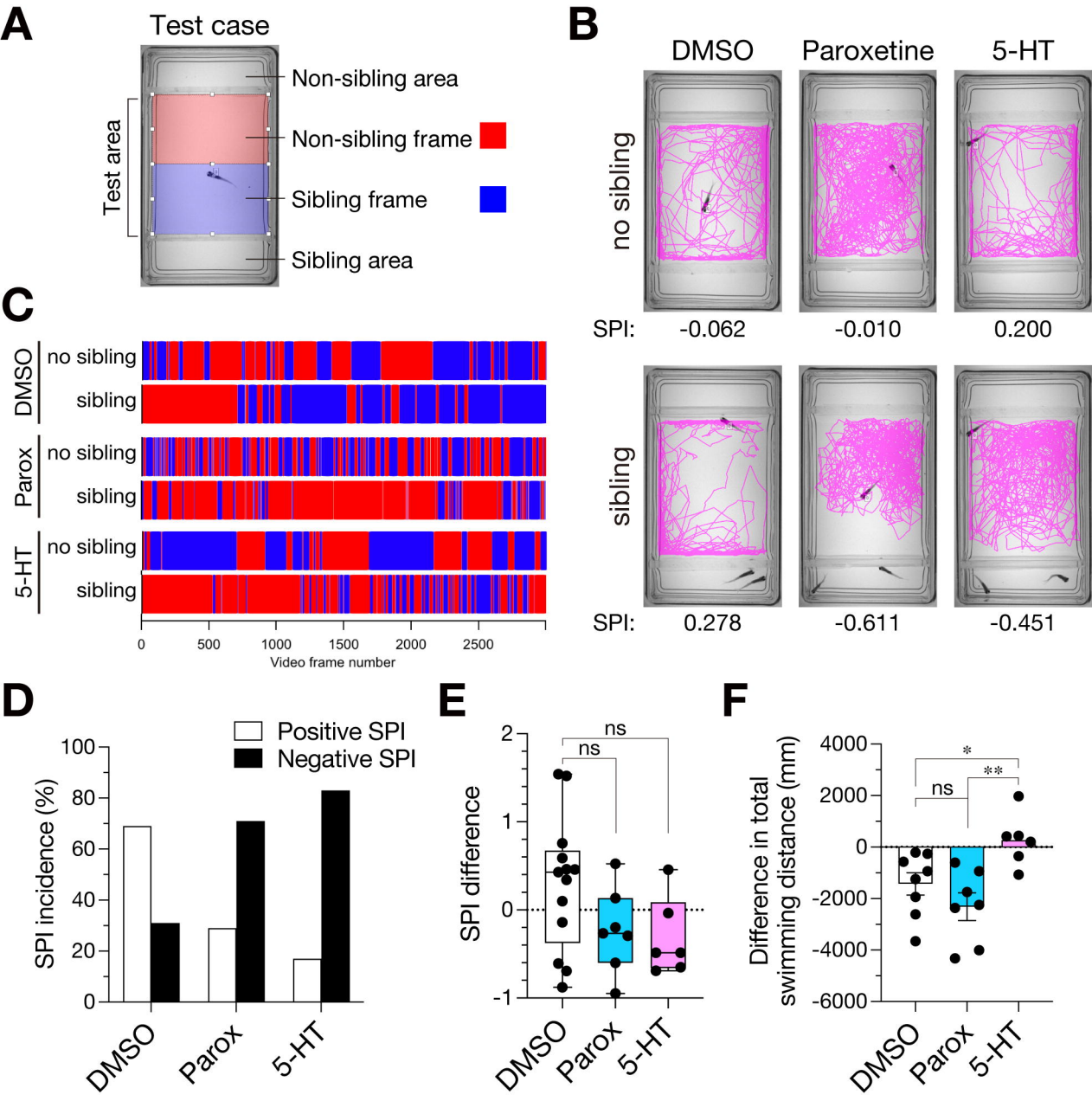
A
Test case
Test area
Non-sibling area
Non-sibling frame
Sibling frame
Sibling area
B
DMSO
Paroxetine
5-HT
no sibling
sibling
SPI:
-0.062
-0.010
0.200
0.278
-0.611
-0.451
C
DMSO
Parox
5-HT
no sibling
sibling
0
500
1000
1500
2000
2500
Video frame number
D
Positive SPI
Negative SPI
SPI incidence (%)
100
80
60
40
20
0
DMSO
Parox
5-HT
E
SPI difference
2
1
0
-1
ns
ns
DMSO
Parox
5-HT
F
Difference in total swimming distance (mm)
4000
2000
0
-2000
-4000
-6000
*
**
ns
DMSO
Parox
5-HT